A PHYSICAL-BIOLOGICAL MODEL OF OʻAHU'S WINDWARD COASTAL WATERS:

IMPLICATIONS FOR LARVAL TRANSPORT

A THESIS SUBMITTED TO THE GRADUATE DIVISION OF THE
UNIVERSITY OF HAWAIʻI AT MĀNOA IN PARTIAL FULFILLMENT
OF THE REQUIREMENTS FOR THE DEGREE OF

MASTER OF SCIENCE

IN

OCEANOGRAPHY

DECEMBER 2016

By

Conor R. Jerolmon

Thesis Committee:

Margaret McManus, Chairperson
Brian Powell
Mark Merrifield
Megan Donahue

ACKNOWLEDGEMENTS

I wish to express my thanks to: The Harold K.L. Castle Foundation Grant #3846 for providing the funding for this research. My advisor, Margaret McManus, along with the other members of my thesis committee: Brian Powell, Mark Merrifield, and Megan Donahue, for all the support and advice that they have provided over the course of this project. The members of Fish Flow: Mark Hixon, Rob Toonen, Erik Franklin, Megan Donahue, Brian Bowen, Margaret McManus, Stephen Karl, Brian Powell, Anna Neuheimer, Chelsie Counsell, Richard Coleman, Mia Kapur, Morgan Winston, Dale Partridge, for making this such an enjoyable project to be a part of.

And all the rest: the McManus Lab: Gordon Walker, Christina Comfort and Daren Martin, the Powell Lab, The Pacific Islands Ocean Observing System, The University of Hawaiʻi Dive Safety Office, as well as the University of Hawaiʻi Department of Oceanography faculty, staff, and students.

TABLE OF CONTENTS

LIST OF TABLES

LIST OF FIGURES

INTRODUCTION

Many marine fish exhibit a pelagic larval stage post spawning (Sale 1991). During this pelagic stage, which may last days to months, depending on the species, larvae may be transported significant distances from their spawning site, a process referred to as larval dispersal (Brothers and Thresher 1985). This process can provide significant challenges to fisheries management as it means that a local population of adults may be derived from an entirely different location. In such a case, management efforts focused on the local population will have little effect on the health of this population. Understanding patterns of larval dispersal is therefore necessary for the proper management and conservation of ecologically and commercially important species (O'Connor et al. 2007). Of particular importance is identifying high self-recruitment areas, which produce larvae that later recruit to that same area.

Attempting to study larval dispersal presents its own set of challenges. While adult and even juvenile fish can be individually marked or tagged and tracked, this approach becomes largely impractical when dealing with the minute size and massive numbers of microscopic larvae (Cowen, Paris and Srinivasan 2006). Because of the inherent difficulties in directly observing/tracking larval dispersal, alternative approaches are typically employed, either with genetics based studies, such as parentage analysis or relatedness studies, or through the use of coupled physical-biological particle tracking models. A physical-biological particle tracking model combines a physical oceanographic model with a particle tracking model that may include a number of additional parameters designed to simulate larval behavior.

The use of physical-biological models for the purposes of studying larval dispersal is still relatively novel, but is becoming increasingly more common. Prior studies using this approach (e.g., Cowen, Paris, and Srinivasan 2006, Cowen and Sponaugle 2009, North et al. 2008, Pfeiffer-Herbert et al. 2007) have primarily focused on dispersal throughout archipelago (or larger) sized regions. This is partly to account for the relatively coarse resolution of the oceanographic models employed (typically 1 km or greater), as these are unable to resolve complex nonlinear interactions in near-shore coastal environments. However, these interactions are likely to influence larval transport and recruitment and impact the self-recruitment capabilities of an area (McManus and Woodson 2012). Prior studies have indicated that self-recruitment may be more important to population dynamics than large scale dispersal patterns (Jones et al. 1999) in many regions. The high resolution model for a bay on the windward side of the island of Oʻahu, Hawaiʻi employed in this study allows for the examination of transport processes on a finer scale than previous efforts. The modeling system implemented in this study is able to more accurately simulate the dynamics of a near-shore region, and provide a better view of larval transport in a small scale coastal environment.

This study was part of a larger project called *Fish Flow*. There are three major components of the Fish Flow project: oceanography, genetics, and ecology. The oceanography and genetics components were designed to determine origin of larvae of commercially important fish in Hawaiʻi and the location of larval settlement utilizing different tools. The ecology component was designed to identify reefs with adult fish populations that are either sources or sinks for the population. After consultation with local fishers, two commonly fished species in

Hawaiʻi – convict surgeonfish (manini [Hawaiian language]; *Acanthurus triostegus*) and goldring surgeonfish (kole; *Ctenochaetus strigosus*) were selected for this project.

The oceanography component of the Fish Flow project examined larval dispersal on the windward coast of the island of Oʻahu, Hawaiʻi, with a particular focus on the Kāneʻohe Bay region. Kāneʻohe Bay is of particular importance from a fisheries management standpoint as it is a region that is both highly productive and heavily fished. There were several major goals of the oceanography component. The first was to attempt to validate the oceanographic models being used to generate current velocity fields for Kāneʻohe Bay and the windward coast regions. The second was to establish overall patterns of connectivity along the windward coast. The third was to establish potential factors that may explain the difference in observed recruitment between the 2014 and 2015 calendar years. The summer of 2014 experienced what was termed by local media as a "biblical" recruitment event (Talbot 2014), while the same period in 2015 experienced abnormally low recruitment (C. Counsell, R. Coleman, M. Donahue, personal communication, 2016). The final goal was to study the physical drivers influencing connectivity in the region. The results of this study are discussed in the following contribution.

METHODS

Study Area

The study area, which covers an area of 1404 km^2 (Figure 1), encompasses Kāneʻohe Bay and the coastal waters on the northeast side of the island of Oʻahu, Hawaiʻi that are exposed to the predominant trade winds. Herein, this area will be described as "windward coastal waters". Kāneʻohe Bay is a semi-enclosed estuarine-bay system on northeast side of the island of Oʻahu; it is the largest sheltered body of water in the Hawaiian Islands (Bathen 1968).

Winds are predominantly northeast trades originating from a semi-permanent region of high pressure to the northeast of the islands. Under trade conditions, which are dominant during summer months from April through September, wind direction in the windward coastal waters may vary from northerly to southeasterly due to the interaction of the northeast trade winds with local terrain (Ostrander 2008). During winter months (October-March) trade conditions still dominate, however passing storm systems and a weakening of the semi-permanent region of high pressure result in an increased frequency of Kona (southwesterly) winds.

Tides in the region are mixed semidiurnal and microtidal, with a mean tidal range of ~0.7 m and maximum range of ~1.1 m (Lowe et al 2009). Tidal frequencies are dominated by the principle lunar semi-diurnal (M2, period of 12.421 hrs.) and principle solar diurnal (S1, period of 24 hrs.) and semi-diurnal (S2, period of 12 hrs.) tidal constituents.

Mean annual rainfall varies between 700 – 1700 mm/year along the coast, generally increasing from south to north, and can exceed 6000 mm/year in the mountains of the Koʻolau

Range which border the coastline and form the watershed for the region (Giambelluca et al. 2013). Rainfall is delivered to the windward coastal waters via direct precipitation, numerous streams along the coastline, and through submarine groundwater seeps. Stream discharge in the region is characterized by extended periods of low flow combined with sporadic periods of high runoff following storm events (DeCarlo et al. 2007).

The windward coastline is bordered by a fringing reef extending 1-2 km from the shore and gently sloping to a depth of 12-13 m. Beyond this depth the slope increases sharply. A fringing/barrier reef (average depth 3-5 m) extends across the mouth of Kāneʻohe Bay and shelters a lagoon area (average depth 10-15 m) containing numerous patch reefs which rise from the lagoon floor to within less than a meter of the surface. The lagoon is connected to the ocean via two main channels, a shipping channel (depth of ~15 m) in the north and the Sampan Channel (depth of ~5 m) in the south part of the bay. The southern-most area of Kāneʻohe bay is a semi-enclosed region that functions almost as a “bay within a bay” (Figure 2).

Oceanographic Model

Ocean current velocity fields were generated using the Regional Ocean Modeling System (ROMS) for the years 2014 and 2015. ROMS is a free-surface, terrain following, primitive equations ocean model (Shchepetkin and McWilliams, 2005). For the windward coast of Oʻahu, a 1 km grid with 30 vertical layers, wind and tidal forcing, at a 3 hr. temporal resolution was used. Open ocean boundary conditions were obtained from the 4 km Hawaiian Islands ROMS model (Matthews, Powell, and Janeković, 2012). The 4 km Hawaiian Islands ROMS regional model is run on a daily basis and incorporates assimilation of available realtime data including

satellite derived sea surface height (SSH), sea surface temperature (SST) and surface currents, along with data from Argo floats, gliders, and high frequency radar. For Kāneʻohe Bay, a 100 m resolution grid with 12 vertical layers, forcing from winds, tides, and stream discharge at a 30 min temporal resolution was used. Topography was created from the 4 m gridded bathymetry of Kāneʻohe Bay made available through NOAA, with minor smoothing applied to average the data onto the 100 m spacing (Figure 2). A constant bottom roughness coefficient was used for the grid. A constant bottom roughness coefficient is not ideal, and will be revised in the future. The windward coast model was used to supply boundary conditions for the Kāneʻohe Bay model.

Atmospheric forcing for the ROMS model was provided by the Weather Research and Forecasting Model (WRF) (Michalakes et al. 2001), tidal forcing from the TPXO tidal model (Egbert, Bennett, and Foreman, 1994), and stream input for Heʻeia, Waiheʻe, Waiāhole, and Waikāne Streams from U.S. Geological Survey stream gage data (USGS 2016).

Particle Tracking Model

Particle motion was studied using the Connectivity Modeling System (CMS)[1] (Paris et al. 2013). CMS is a Lagrangian particle-tracking model that employs a 4th order Runge-Kutta scheme to transport virtual particles through a set of velocity fields. Particles were set to be neutrally buoyant and passively advected throughout each simulation. Particles intersecting an open ocean boundary (labeled 1, 2, 3 in Figure 1b) were considered lost from the simulation. The 'avoidcoast' flag was set to prevent particles from becoming stranded on land. This setting causes particles that cross shoreline boundaries to be returned to their previous location and

1 A description of all of the particle-tracking models considered for this study is given in APPENDIX A

moved with reduced velocities or held in place to keep them in the water (Paris et al. 2013). The 'upperlevelsurface' flag was likewise set to prevent particles from passing through the sea surface. The Seascape Module was employed to designate habitat areas on the grids, which would function as release and settlement locations for the particles. The CMS was chosen for this project primarily for its ability to work with nested grids. Limitations of the CMS include requiring fixed depth levels and orthogonal (x=E, y=N) grids. Both of these limitations had to be addressed as ROMS uses terrain following stretched vertical coordinates and both the windward coast and Kāneʻohe Bay grids were rotated 45 degrees relative to the cardinal directions.

In order to address the fixed depth requirement of the CMS, the ROMS model output was first converted to fixed depth levels using an objective analysis using weighted decorrelation scales. Depths were set to [0, 0.5, 1.0, 1.5, 2.0, 2.5, 3.0, 3.5, 4.0, 4.5, 10.0, 15.0] m for Kaneohe Bay and [0, 2, 4, 6, 8, 10, 20, 30, 40, 50, 100, 200] m for the windward coast. These depths were chosen as they best represented the average depths of the original stretched layers. A coordinate rotation was performed on each grid in order to satisfy the orthogonality requirement of the CMS. The x and y position of each point on each grid was first converted to a distance from a 0 point (the lower left corner of the windward coast grid) and then scaled to equivalent longitude and latitude about the equator. The 3 hr. windward coast output was then linearly interpolated to 30 min to match the Kāneʻohe Bay model output.

Habitat polygons representing source and sink locations were defined based on the benthic habitat maps created by NOAA's National Centers for Coastal Ocean Science (NCCOS) (BAE 2007) (Figure 3a). The NCCOS habitat shapefiles were read into QGIS. The hard substrate types were then merged and a 100 m buffer added to account for the 100 m Kāneʻohe

Bay model resolution. Particle release locations were at the centroid of each polygon. If the centroid of a polygon was on land, then the release location was redefined so as to be in the water. Release depth was set to 3 m for all locations, based on observations of manini spawning aggregations (Schemmel and Friedlander 2016, in prep). If the model depth at the release site was less than 3 m, then the release point was set to half the depth at that location. Habitat polygons were combined to define specific areas of interest within the study area. These specific areas of interest include the North Coast (polygons 1-8), Mid Coast (polygons 9-16), Reef Flat (polygons 17-23), North Bay (polygons 24-25), Mid Bay (polygons 26-33), South Bay (polygons 34-38), Inner Bay (polygons 39-44), Mokapu (polygons 45-47), and South Coast (polygons 48-54) (Figure 3b,c).

The turbulence module of the CMS was used to simulate particle motion on scales smaller than the grid resolution. The module is used to perturb each particle in a random direction at a specified interval at a velocity proportional to a specified dispersion constant. The horizontal dispersion coefficient used for the Kāneʻohe Bay grid was 0.2 m^2/s, after Lowe et al. (2005). For the windward coast grid, a value of 2 m^2/s was used to account for the lower (by a factor of 10) resolution of the grid. As CMS requires a single value (per grid) for vertical dispersion, rather than depth varying profile, a value of 0.001 m^2/s was used for both grids. This value represented the average vertical dispersion coefficient in a turbulence model comparison study by Durski et al. (2004). The turbulence timestep was set equal to the model timestep at 300 s.

The parameters of larval release for this study are based on two commonly fished species: convict surgeonfish (manini [Hawaiian language]; *Acanthurus triostegus*) and goldring

surgeonfish (kole; *Ctenochaetus strigosus*). Manini and kole have been observed to follow a semi-lunar spawning cycle, spawning during afternoon ebb tides around the new and full moons (Randall 1961, Lobel 1989, Schemmel and Friedlander 2016, in prep). To simulate this behavior, particle release times were set to 03:00 UTC (17:00 HST -1 day) for new and full moons between January 2014 and October 2015. A total of 46 model simulations were run, with 1000 particles simultaneously released from each polygon for a total of 54,000 particles released per simulation (Table 1). Each simulation was set to run for 65 days, with particles being allowed to 'settle' into individual polygons after 55 days. In other words, after 55 days had elapsed within a simulation, any particle within or entering a polygon would stop in that location, and be considered to have successfully settled to that location. These timings were chosen based on manini pelagic larval duration estimates of 54-72 days (Longnecker and Langston 2008, Randall 1961).

Settlement, Retention, and Connectivity

Within this text, the terms “settlement,” “retention,” and “connectivity” will be used with specific meanings. “Settlement” will be used to describe the percentage of total number of particles released during a simulation that settle in a particular polygon or area. “Retention” will describe the percentage of particles released from a particular polygon or area that settle within the model domain by the end of the simulation (i.e., that are not lost through a boundary or stranded offshore). “Connectivity” will describe the percentage of particles released from a particular polygon or area that settle in another specific polygon or area.

Instrumentation Deployed

Instruments were deployed in Kāneʻohe Bay and the adjacent shelf at four different sites over the course of the study (Figure 1b). The data from these instruments were compared to simulation output from the numerical model as a check of the accuracy of the model.

Site A, in central Kāneʻohe Bay, was located at 21.45760º North, 157.80683º West. The site was on a dome shaped patch reef, ~37 m diameter at the surface, rising from the bay floor at ~12 m depth. The upper 1.5 m of the dome had high coral cover (exceeding 90%). Coral cover declined between 1.5 and 4 m, although at this site sparse coral coverage continues to depths of 9-10 m.

Site B was located on another patch reef in the northern part of Kāneʻohe Bay at 21.47528º North, 157.82993º West. This reef was also roughly dome shaped, ~38 m diameter at the surface. Coral distribution follows a similar pattern to Site A, with high coral cover at depths less than 1.5 m, declining coral cover between 1.5 m and 4 m, and very sparse to nonexistent coral cover greater than 4 m depth, where the substrate is comprised almost entirely of broken coral fragments and loose sediment.

Site C was located east of Kaʻaʻawa on the 12 m isobath at 21.56641º North, 157.84360º West, while Site D was located east of Lanikai and just north of Moku Nui on the 12 m isobath at 21.39939º North, 157.69925º West. Both of these locations were characterized by a limestone pavement substrate with algal cover and occasional coral and sand patches.

Instrumentation deployed within Kāneʻohe Bay included 6 thermistors and one current meter. In order to measure water column stratification, three Seabird Electronics SBE39

thermistors were deployed at Sites A and B at 1 m, 2 m, and 4 m depths (Figure 1b). Each thermistor measured water temperature at 2-minute intervals. A Nortek Aquadopp current meter was also deployed at Site B at a 2 m depth on the northeast side of the patch reef. The sensor measured currents at a single point using a 30-second average every 2 minutes. The blanking distance for the acoustics was set at 4 meters horizontally from the sensor so that the sensor was sampling currents at a point 2 m deep and ~4 m off of the reef slope. All sensors were deployed on April 3, 2015. Each sensor was mounted on a cinder block, weighted down with ~25 lbs. of anchor chain, and deployed using SCUBA. The Nortek sensor was briefly retrieved and redeployed on June 4, 2015 for a battery change, and recovered on July 16, 2015. All six thermistors were retrieved and redeployed on October 28, 2015 for battery changes. The thermistors were recovered on April 5, 2016.

Sontek ADPs were deployed at Sites C and D on March 24, 2015 and May 4, 2015 respectively. Both sensors were configured to measure current velocity profiles over twelve 1-meter intervals from one meter above the seafloor to the surface. Current velocities were averaged over 30 seconds, with a sampling interval of 2 minutes. Each sensor was attached to a tripod mount, and weighted down with ~70 lbs. of lead and iron weights. The sensor at Site C was recovered on July 21, 2015. The sensor at Site D was recovered on July 28, 2015. Deployment and recovery at both sites was done off of a small craft (28 ft. whaler) through the use of SCUBA.

Comparison of Oceanographic Model Output and Observational Data

For the purposes of comparing the ROMS model output to the observational data, in each case the ROMS data were taken from the grid cell containing the latitude and longitude coordinates of the instrument. For the temperature and point velocity measurements, ROMS data were taken from the depth level closest to the instrument depth at time of deployment. In the case of the ADP velocity profiles, both instrument and ROMS velocity data were integrated over the height of the profile.

Sea surface height (SSH) data were only available (as pressure) from the ADP instrument deployed at Site C, so comparison was restricted to this location in the Windward Coast ROMS model. An estimate of 'model skill' (Warner et al. 2005) also referred to as 'index of agreement' (Willmott 1981) was calculated according to the formula

$$Skill = 1 - \frac{\sum \left| X_{model} - X_{obs} \right|^2}{\sum \left(\left| X_{model} - \bar{X}_{obs} \right| + \left| X_{obs} - \bar{X}_{obs} \right| \right)^2}$$

in order to compare each measured variable X_{obs} with the model prediction X_{model}. Skill is on a scale of 0 to 1, with 1 indicating perfect agreement and 0 indicating perfect disagreement.

RESULTS

Comparison of Oceanographic Model Output and Observational Data

A comparison of the time-series of modeled and observed SSH at Site C (Figure 4a) shows a very good match, with the two SSH time-series appearing in phase and the model perhaps just slightly underestimating the overall variability at this location. Model skill is excellent at 0.943 (Table 2). A comparison of spectra of modeled and observed SSH at Site C (Figure 4b) shows most of the energy at 1.0 and 1.93 cycles per day (0.0417 and 0.0804 cycles per hour), corresponding to the frequencies of the primary tidal constituents (S1 and M2, respectively) as expected. Agreement between the model and observations is again quite good, with the model accurately capturing both the width and height of both peaks, although slightly underestimating the energy outside of the two main peaks.

A time series of depth integrated along and cross-shore currents at Site D (Figure 5a,b) also displays a reasonably good agreement between the model and observations. Variability in the along-shore (u) direction (Figure 5a) in particular appears to have been captured quite well by the model (skill of 0.662). However, model agreement with the observational data is less good in the cross-shore direction (Figure 5b) with a model skill of only 0.171. Additionally, the observational data displays significant high frequency variability in the cross-shore direction that is not resolved by the 3 hr. model resolution. It should be noted however that cross-shore velocities (at ~5 cm/s) in this area are 2-4 times weaker than along-shore velocities (at 10-20 cm/s). A comparison of the rotary spectrum (Figure 5c) of the observed and modeled currents again shows relatively good agreement, with the model accurately capturing the energy in the

M2 tidal frequency and its first harmonic. The model does slightly overestimate the energy in the S1 tidal frequency and again underestimates the energy in the frequencies between the two main peaks.

A time series comparison of along-shore and cross-shore currents at Site B (Figure 6a,b) displays reasonable agreement between the model and observational data. The model consistently underestimates current strength, particularly in the cross-shore direction. The model also fails to capture a prominent directional shift that occurs between April 20 and 28, although it does capture some of the increased variability that also occurs during this period. Model skills are 0.374 and 0.353 for along and cross-shore currents respectively (Table 2). The rotary spectrum for this location (Figure 6c) also shows peaks at the S1 and M2 frequencies (1.0 and 1.93 c.p.d. / 0.0417 and 0.0804 c.p.h.), as expected. However, the S1 and M2 peaks are not well defined in the observational data as the energy is much more spread out than at the other locations. The model shows more sharply defined peaks at these frequencies, and again slightly underestimates the overall energy.

Current ellipses plotted for Sites B, C, and D (Figure 7) show good agreement between the model and observations for the two locations outside the bay (Sites C & D), with similar length of major and minor axes, and similar orientation. Major axes for all ellipses were primarily oriented along-shore, with the ellipses for the observed currents having a slight cross-shore component (more prominent at Site D). Current ellipses for Site B within the bay do not match well, with the ellipse from observed currents being larger (as a result of the stronger currents as noted above), and rotated ~55^{o} relative to the model current ellipse.

Surface temperatures[2] at Sites A and B compare very well between the model and observations, with the model capturing the annual variability nearly exactly (Figure 8). The daily variability, including the (near) daily temperature inversion in the upper 4 m, is also captured reasonably well (Figure 9). There does appear to be a temperature bias of +1.5 ^{o}C that persists throughout the model output, however. Correcting for this bias moves the average model skill for temperature from 0.799 (already good) to an excellent value of 0.975 (Table 2).

Settlement and Retention Patterns

Over the 46 particle tracking simulations, overall retention rates varied between 14.29% and 35.35%. Settlement rates were highest in the Inner Bay area (average of 16.9%) and South Bay areas (average of 4.07%). Average settlement in other areas of Kāneʻohe Bay was between 1% (Mid Bay) and 2.5% (North Bay). Settlement rates in all areas outside of the bay averaged less than 1% (Table 2).

Connectivity grids created from the simulations show consistently high rates of settlement and retention in southern Kāneʻohe Bay (polygons 34-44) particularly in the Inner Bay area (Figures 10-13). High settlement rates are also seen in the North Bay area, although with less consistency. This can be seen in Figures 12 and 13 where the January 20, 2015 simulation shows relatively low settlement in the North Bay area, while significantly higher settlement can be seen in the same area for the April 4, 2015 simulation. The Mid Bay and Reef Flat show relatively low rates of settlement but moderate retention, suggesting that these areas are primarily seeding other areas of the bay. Settlement and retention rates are both significantly

2 An additional analysis of the temperature data collected at Sites A and B is included in APPENDIX B.

lower for areas along the coast outside of the bay (polygons 1-16 and 45-54). Connectivity averaged over the 2014 and 2015 calendar years does not reveal any significant differences between these two years (Figures 10, 11).

Temporal Changes in Settlement and Retention

Throughout the simulations, settlement in the Inner Bay area is substantially higher than all other areas of Kāneʻohe Bay, with the exception of a large dip in settlement in the January 2014 simulations (Figure 14a). Settlement in other areas of the bay is generally consistent throughout the simulations, with the exception of the North Bay, which exhibits peaks in settlement in the May 2014 and March-April 2015 simulations (Figures 14a, 15a). Retention rates are also highest in the Inner Bay area, and tend to decrease toward the north (Figure 14b). Retention rates for the Mid Bay, South Bay and Inner Bay areas also show a dip in January 2014, corresponding to the dip in Inner Bay settlement, while retention for the Reef Flat, North Bay and Mid Bay areas exhibits peaks in May 2014 and March-April 2015 corresponding with the peaks in North Bay settlement (Figures 14, 15).

Particle Loss at Grid Boundaries

The loss of particles through each of the 3 grid boundaries (Northwest, Northeast and Southeast) is depicted in Figure 16. Each of the panels in Figure 16 represents loss through a different boundary: Northwest, Northeast, and Southeast (labeled 1, 2, & 3 respectively in Figure 1). Within each panel of Figure 16, rows represent independent model runs and columns represent polygons, with the color of each grid cell representing the percentage of particles lost

from that polygon through that grid boundary for that model run. The majority of losses are in the along-shore direction, either through the Northwest or Southeast boundaries. Comparatively few particles are lost in the cross-shore direction through the Northeast boundary. The plots show high loss rates, often greater than 95%, for particles released outside Kāneʻohe Bay (the North Coast, Mid Coast, Mokapu, and South Coast areas), with particles released north of the bay typically leaving the model domain through the Northwest boundary and particles released south of the bay typically leaving the model domain through the Southeast boundary. Notable exceptions to this pattern include simulations 1-5 (January - March 2014), 26-27 (January - February 2015) and 37 (July 2015), which are dominated by losses through the Southeast boundary and exhibit relatively high losses from Kāneʻohe Bay. The mid sections of the Northwest and Southeast grids (representing particle loss from particles released within the bay area) appears to show a periodicity of 4-5 lunar cycles, indicating a reversal of alongshore transport direction on this timescale.

Regression Analysis

In an attempt to isolate the primary driving factors influencing changes in connectivity, that act over periods of weeks-months, variations in settlement and retention for each area (defined in the Methods section) were correlated against a number of potentially related environmental variables, with the results displayed in Tables 3a and 3b. North and Mid Windward Coast retention is not well correlated with any of the environmental variables (all |r-values| <0.5). North Coast retention shows weak correlation with cross shore winds and upper 3m cross shore currents into the bay, while Mid Coast retention shows similarly weak correlation

with along-shore winds and 10 day cross shore winds. Retention in the Kāneʻohe Bay Reef Flat area likewise exhibits at best weak correlations with all environmental variables, with the strongest being the upper 3m cross-shore currents into the bay. Retention in both the North and Mid Bay areas shows moderate to strong (|r-values| between 0.5 and 0.7) correlation with both along and cross-shore winds (total and 10 day). Retention for both the South and Inner Bay areas show high correlation with the SSH gradient angle ($|r|>0.7$), with South Bay retention also showing high correlation ($r=0.67$) with the along-shore SSH gradient. Retention for the Mokapu area is essentially uncorrelated with any of the environmental variables. This is also the case for retention for the South Coast area, with the exception of moderate correlation with 10-day cross-shore winds.

Settlement in all areas outside Kāneʻohe bay shows little to no correlation with any of the environmental variables examined. Within the bay, the settlement in the Reef Flat area also exhibits little to no correlation with any of the environmental variables. Settlement in the North Bay area shows moderately strong correlation with both along and cross-shore winds ($r=-0.7$ and -0.58 respectively). Settlement in the Mid Bay is essentially uncorrelated with any environmental variable, while South Bay settlement shows a moderate correlation with cross-shore winds ($r=-0.57$), upper 3m cross-shore currents into the bay ($r=-0.52$), and flux out of the Inner Bay ($r=0.52$). Settlement in the Inner Bay area is highly correlated with the SSH gradient angle ($r=0.72$) and moderately correlated with the along-shore SSH gradient ($r=0.57$) and flux out of the Inner Bay ($r=-0.6$).

DISCUSSION

Comparison of Oceanographic Model Output and Observational Data

The ROMS oceanographic model performed well in matching observational data in most cases. SSH and temperature were modeled exceptionally well (skill>0.9), while along-shore currents outside of Kāneʻohe Bay at Sites C and D also showed reasonably high agreement with observations (skill~0.6), especially considering the relatively coarse model resolution at 1 km and the moderately complex actual topography (such as the 2 small islands just south of Site D that were unresolved by the model).

The model performed less well in reproducing the currents at Site B in Kāneʻohe Bay (skill~0.36). One factor that may have contributed to this decrease in performance was the deployment location of the sensor on a 38 m diameter patch reef, the size of which is significantly less than the 100 m model resolution making this reef essentially undetectable to the model. However, the presence of the patch reef almost certainly influenced currents in the vicinity. Observations at this site were also limited to a single point, rather than a profile, making a generalized comparison more difficult. The omission of certain forcing terms, such as wave forcing across the reef crest and reef flat also likely affected the model performance in this area.

Waves

An additional consideration when examining Kāneʻohe Bay currents would be the lack of wave forcing (omitted due to computational limitations) in the physical model. Previous studies

(Hearn and Atkinson 2001, Lowe et al. 2009) have indicated that wave forcing has significant influence on the current dynamics of barrier reef systems including Kāneʻohe Bay. These studies show that waves breaking over the reef crest set up a mass transport across the reef flat, which in turn sets up a pressure gradient that drives a return flow out of the channels. At least some of this return flow angles back out over the reef slope, where it is then forced back over the reef crest and reef flat, and is effectively recirculated through the bay. Along with streamflow into the bay, wave forcing is a major factor in determining the flushing rate of the bay, with larger waves resulting in greater wave forcing and higher flushing rates (Hearn and Atkinson 2001).

The discrepancy between the observed and modeled currents at Site B does show a significant correlation (p-value $<10^{-5}$) with wave heights measured just outside of Kāneʻohe Bay, although the correlation is not particularly strong ($r=0.47$ and $r=0.39$ for along-shore and cross-shore currents respectively) (Figure 17). This would indicate that while wave forcing is likely contributing to the discrepancy between the model and observations, other factors (such as the effect of small patch reefs on the currents) are also at play.

The extent to which the addition of wave forcing to the model would affect connectivity in the region would depend on the amount of wave driven flow across the reef flat that is effectively flushing the lagoon area of the bay. Results from the Lowe at al. 2009 study have indicated that this effect is substantial, with residence times of particles in the lagoon of less than a week; while in our study particles might remain in the lagoon area for a month or more. Overall, settlement and retention rates within Kāneʻohe Bay would be expected to be significantly lower if wave forcing were included in the model.

Settlement and Retention Patterns

Overall patterns of connectivity are dominated by settlement and retention within Kāneʻohe Bay (Figures 10-12). The bay itself tends to act as a kind of trap, with particles released within or entering the bay having a much higher chance of being retained for the full model run. Particles released outside of the bay have a very high chance of leaving the grid (by intersecting the model boundaries) within the first 2 weeks of the 65-day simulation. Surface currents with a strong onshore component early in the simulation would tend to push particles released on the Reef Flat area and possibly areas outside the bay into the lagoon area or the bay, where they would be more likely to be retained. If these currents were the result of onshore winds, that could explain the moderate correlation between overall settlement and 10 day cross-shore winds (Table 3a).

Net currents along the windward coast can be strong enough that particles exiting the bay may leave the grid in either along-shore direction in as little as 48 hours. As a result, settlement in the North Coast, Mid Coast, Mokapu and South Coast areas is primarily dependent on timely release of particles from the bay (a few days before the end of the pelagic larval stage), and the prevailing along-shore currents at this time. This is particularly true for areas north of the bay. South of the bay, particles may be trapped against the southern edge of Mokapu Point during trade wind conditions, or within the eddy that occasionally forms in this area.

Temporal Changes in Settlement and Retention

Within the bay, variations in overall settlement rates appear to be primarily affected by variations in settlement rates in the North and Inner areas of Kāneʻohe Bay. Peaks in overall

settlement tend to correspond with peaks in North Bay settlement and North Bay, Mid Bay and Reef Flat retention (Figure 15). This would suggest that these periods of increased settlement were the result of a greater percentage of particles from the North and Mid Bay and Reef Flat areas settling in the North Bay area during these times. A time series of connectivity between these areas (Figure 18a) exhibits peaks at these same times (May 2014 and March-April 2015) and so supports this hypothesis. The dip in overall retention in early 2014 appears to correspond with a decrease in settlement in the inner bay area along with below average retention for all areas of the bay, most prominently in the South, Mid and Inner Bay areas. A time series of connectivity between these areas (Figure 18b) suggests that this initial dip was the result of a reduced number of particles from the South, Mid and Inner Bay areas settling in the inner bay area in these simulations.

While one goal of this study was to explain the large difference in recruitment observed between the 2014 and 2015 calendar years, the high degree of similarity between 2014 and 2015 connectivity patterns (Figures 10, 11) suggest that this difference was primarily based on biological (rather than physical) factors, and/or as a result of factors outside of the model grid. It seems likely that the difference was due to either a change in spawning behavior (number of larvae released), or in a change in current patterns outside the model grid bringing in larvae from another location.

Particle Loss at Grid Boundaries

Particle loss is primarily in the along-shore direction due to the predominance of along-shore currents along the coast. The tendency for particles released from the North and

Mid Coast areas to escape through the Northwest boundary and particles released from the Mokapu and South Coast areas to escape through the Southeast boundary is partially explained by the limitations of the model grid: once a particle intersects a boundary it is effectively lost, as the model has no information for anything that occurs outside of the grid. Therefore once a particle exits the model domain it cannot re-enter, even if currents at the boundary were to reverse direction, as happens frequently with tidal currents. It is possible that the periodic reversals in net alongshore transport direction occurring at timescales of 4-5 lunar cycles could be due to the interaction of mesoscale eddies with the Hawaiian coastline. More research on this hypothesis would be necessary to draw a definitive conclusion.

Regression Analysis

Local winds appear to have a strong effect on connectivity throughout the region. Correlations between wind vectors and retention (Figure 19 and Table 3a,b) suggest that current patterns within the bay under strong trade wind conditions tend to trap particles, particularly from the North Bay, Mid Bay, and Reef Flat areas, in the Northeastern most part of the bay (North Bay area). This phenomenon can be observed in animations of the particle motions. Similarly, sustained cross-shore winds also appear to help trap particles in the South Bay area (Figure 20).

Retention and settlement across the study area is by far the highest in the southeastern most part of Kāneʻohe Bay (Inner Bay area). The high settlement and retention rates appear to be due to the limited exchange between this area and the rest of Kāneʻohe Bay. This is supported by the Lowe et al. (2009) study, which found significantly higher particle retention periods (1-2

months) for the Inner Bay area when compared to the rest of the bay (1-6 days). Changes in settlement and retention rates in this area are then likely affected primarily by the rate of exchange with the main bay area.

Exchange across the mouth of the inner bay appears to be primarily controlled by the direction of the SSH/pressure gradient in this area. Under typical conditions, northeasterly trade winds combined with outflow from Heʻeia Stream appear to "pile up" water in the Heʻeia area resulting in a pressure gradient angled ~45^{o} across the mouth of the inner bay. Under these conditions the wind forcing acts in direct opposition to the pressure gradient force, resulting in weak surface currents directed parallel to the inner bay mouth and limiting exchange across this boundary (Figure 21a). However, changes in wind strength and direction and stream outflow can affect the direction of the pressure gradient, which appears to function as a kind of "gate". As the gradient rotates toward the cross-shore direction and the isobars become perpendicular relative to the mouth of the inner bay, the gate effectively opens, resulting in surface currents directed out of the inner bay and allowing more particles to escape into the main bay (Figure 21b). The gradient can also swing in the other direction, pointing into the mouth of the inner bay, further limiting the ability of particles to escape from this area (Figure 21c). The exact mechanism controlling the direction of the gradient is unclear, although it seems likely to be related to both wind direction and stream outflow. Interestingly, both extremes in direction occurred at the same time of year, with the extreme "open" state occurring in January - February 2014, and the extreme "closed" in January - February 2015. Both cases occurred during weak/non-trade conditions with average streamflow slightly higher during the 2014 event.

One additional consideration in regard to exchange between the Inner Bay and the main bay is that the oceanographic model does not include forcing due to discharge from Kaneohe Stream. Kaneohe Stream outflows directly into the southern part of the Inner Bay, and this discharge would almost certainly affect the pressure gradient in this area. The likely result of including this forcing would be a rotation of the pressure gradient toward the “open” direction, which should reduce the residence time of particles in the Inner Bay, resulting in reduced retention and settlement in this area.

Based on these simulations, winds appear to be the most important factor affecting variations in the distribution of particles in the windward coastal waters and particularly in Kāneʻohe Bay. A general weakening of or change in direction away from the typical trade wind regime would potentially affect connectivity by allowing more particles to escape the bay, leading to lower overall retention, and particularly affecting the North Bay area in terms of reduced settlement.

CONCLUSIONS

A coupled physical-particle tracking model was used to simulate the transport of larvae of two commonly fished species in Hawaiʻi – convict surgeonfish (manini [Hawaiian language]; *Acanthurus triostegus*) and goldring surgeonfish (kole; *Ctenochaetusstrigosus*) for the years 2014 and 2015.

The oceanographic model performed well overall in comparison with observations. Model skill for currents at Site B within Kāneʻohe Bay was less than ideal however. Key additions to the model that should improve performance would be: wave forcing, stream discharge from Kāneʻohe Stream, and a non-uniform bottom roughness coefficient.

While one goal of this study was to explain the large difference in recruitment observed between the 2014 and 2015 calendar years, the high degree of similarity between 2014 and 2015 connectivity patterns, despite the vast differences in numbers of larvae recruited, suggest that this difference was primarily based on biological (rather than physical) factors, and/or as a result of factors outside of the model grid.

The overall patterns of connectivity for the entire model grid are dominated by settlement and retention within Kāneʻohe Bay. Within Kāneʻohe Bay, settlement rates are highest in the Inner Bay area, while settlement variability is highest in the North Bay and Inner Bay areas. Based on model simulations, winds appear to be the most important factor affecting settlement rates in the North Bay and South Bay areas. Exchange across the mouth of the inner Bay appears to be primarily controlled by the direction of the SSH/pressure gradient in this area.

As previously mentioned, this modeling work is part of a larger project named ‘Fish Flow’. There are three major components of the *Fish Flow* project (Oceanography, Genetics, and Ecology). The project was intended to run from 2015-2016, however, because the summer of 2015 was an abnormally low fish recruitment season, the genetics and ecological components of the projects were unable to sample sufficient fish to accomplish their planned analyses. The ‘Fish Flow’ team will add samples from the summer of 2017 to the samples from the summer of 2016, which was a more normal recruitment season. A detailed comparison of oceanographic, genetic and ecological data will therefore occur in subsequent work.

TABLES

Table 1: Simulations listed by simulation start date. Columns are: simulation start / particle release time (UTC), lunar phase, percentage of total particles released that were retained in the windward coastal waters, and percentage of particles which settled in each area of the windward coastal waters.

Simulation Start	Moon phase	% Retained	% Settled North Coast	% Settled Mid Coast	% Settled Reef Flat	% Settled North Bay	% Settled Mid Bay	% Settled South Bay	% Settled Inner Bay	% Settled Mokapu	% Settled South Coast
01/01/2014 03:00:00	New	18.770	0.028	0.115	0.819	0.102	1.019	3.926	9.306	0.587	2.870
01/16/2014 03:00:00	Full	14.639	0.111	0.115	1.463	0.263	1.406	3.470	6.589	0.607	0.615
01/30/2014 03:00:00	New	14.287	0.204	0.411	0.972	1.087	0.441	3.750	6.713	0.383	0.326
02/14/2014 03:00:00	Full	16.269	0.200	0.365	0.791	1.065	0.613	3.991	8.594	0.428	0.222
03/01/2014 03:00:00	New	23.672	0.078	0.109	0.646	2.626	0.459	6.035	13.161	0.274	0.283
03/16/2014 03:00:00	Full	32.333	0.037	0.122	3.011	1.689	1.902	4.935	19.841	0.517	0.280
03/30/2014 03:00:00	New	31.374	0.244	0.400	2.374	0.674	1.274	4.039	20.157	1.076	1.135
04/15/2014 03:00:00	Full	32.024	0.122	0.217	1.787	1.331	1.181	3.948	22.320	0.415	0.702
04/29/2014 03:00:00	New	28.341	0.089	0.322	1.287	1.704	1.017	3.319	20.211	0.144	0.248
05/14/2014 03:00:00	Full	29.367	0.261	0.491	0.609	2.907	0.578	4.004	19.967	0.294	0.256
05/28/2014 03:00:00	New	34.869	0.139	0.439	0.598	7.685	0.524	3.872	21.046	0.252	0.313
06/13/2014 03:00:00	Full	31.354	0.200	0.315	0.819	5.370	0.309	3.654	20.056	0.307	0.324
06/27/2014 03:00:00	New	29.170	0.052	0.070	1.269	4.533	1.411	2.654	18.580	0.280	0.322
07/12/2014 03:00:00	Full	27.163	0.085	0.372	0.722	2.983	1.387	2.563	18.420	0.317	0.313
07/26/2014 03:00:00	New	26.524	0.150	0.515	1.400	2.348	1.365	2.883	17.326	0.267	0.270
08/10/2014 03:00:00	Full	27.322	0.004	0.211	1.119	1.765	1.552	3.419	18.502	0.287	0.465
08/25/2014 03:00:00	New	26.991	0.181	0.319	0.446	2.324	1.270	4.772	17.089	0.428	0.161
09/09/2014 03:00:00	Full	29.500	0.380	0.272	1.407	3.863	0.837	4.359	17.337	0.774	0.270
09/24/2014 03:00:00	New	29.187	0.163	2.006	1.607	2.750	1.380	3.274	17.774	0.131	0.102
10/08/2014 03:00:00	Full	26.420	0.654	0.272	0.761	3.663	0.369	3.285	17.219	0.152	0.046
10/23/2014 03:00:00	New	24.774	0.111	0.435	0.869	2.872	0.322	3.504	16.309	0.261	0.091
11/06/2014 03:00:00	Full	28.583	0.213	1.767	2.057	0.678	1.287	3.148	19.172	0.176	0.085
11/22/2014 03:00:00	New	24.750	0.507	0.419	1.015	0.846	2.500	2.987	15.969	0.380	0.128
12/06/2014 03:00:00	Full	30.474	0.087	1.374	1.624	1.554	1.752	3.056	19.909	0.761	0.357
12/21/2014 03:00:00	New	26.087	0.052	0.924	1.130	0.722	1.356	2.520	18.459	0.352	0.572
01/05/2015 03:00:00	Full	28.169	0.169	0.411	1.715	0.561	1.987	3.494	18.985	0.622	0.224
01/20/2015 03:00:00	New	23.626	0.635	0.944	0.506	0.902	0.813	2.711	16.956	0.072	0.087
02/03/2015 03:00:00	Full	22.044	0.100	0.150	1.152	1.059	0.380	3.139	15.470	0.406	0.189
02/18/2015 03:00:00	New	25.443	0.000	0.056	1.574	2.724	1.546	5.469	13.763	0.220	0.091
03/05/2015 03:00:00	Full	26.181	0.085	0.494	1.476	4.650	1.370	5.709	11.689	0.554	0.154
03/20/2015 03:00:00	New	34.454	0.089	0.189	1.113	11.443	0.581	8.200	12.144	0.420	0.274
04/04/2015 03:00:00	Full	35.346	0.494	0.894	2.059	6.657	1.991	5.515	17.659	0.046	0.030
04/18/2015 03:00:00	New	31.867	0.039	0.035	3.122	3.670	2.285	5.480	16.322	0.463	0.450
05/03/2015 03:00:00	Full	30.981	0.004	0.007	1.657	2.281	1.744	5.250	19.446	0.400	0.191
05/18/2015 03:00:00	New	26.133	0.000	0.093	1.444	0.406	1.231	4.370	18.306	0.170	0.113
06/02/2015 03:00:00	Full	24.733	0.015	0.083	1.407	0.600	1.004	3.715	17.578	0.154	0.178
06/16/2015 03:00:00	New	27.143	0.037	0.119	1.081	1.337	0.787	3.424	19.589	0.322	0.446
07/01/2015 03:00:00	Full	25.226	0.241	0.383	2.124	1.472	0.711	2.702	17.254	0.248	0.091
07/15/2015 03:00:00	New	26.841	0.617	0.593	2.606	0.624	1.269	2.804	16.985	1.159	0.185
07/31/2015 03:00:00	Full	25.781	0.056	0.069	1.765	0.672	1.369	3.243	17.194	0.541	0.874
08/14/2015 03:00:00	New	19.839	0.067	0.211	1.024	0.707	1.085	2.524	13.380	0.474	0.367
08/29/2015 03:00:00	Full	22.600	0.270	0.304	1.846	0.774	0.837	3.483	14.322	0.415	0.348
09/13/2015 03:00:00	New	31.100	0.470	0.809	2.393	1.719	1.746	5.952	16.744	0.609	0.657
09/28/2015 03:00:00	Full	30.078	0.250	0.370	2.133	3.276	1.374	7.419	14.320	0.426	0.509
10/13/2015 03:00:00	New	28.215	0.174	0.835	2.272	3.326	0.730	5.400	14.752	0.374	0.352
10/27/2015 03:00:00	Full	26.061	0.443	0.546	1.387	5.648	1.111	6.302	10.272	0.150	0.202

Table 2: Model skill and root-mean-square error (RMSE) from comparing modeled predictions to observations at each site. Along and cross-shore current skills and RMSE for Sites C and D are from depth integrated currents. Temperature skill and RMSE represents the average of the 6 sensors deployed at Sites A and B. Adjusted temperature skill and RMSE were calculated after adding a -1.5 ºC correction to the model output.

	Model Skill	**RMSE**
SSH (Site C)	0.943	7.62 cm
Along-shore currents (Site C)	0.593	12.77 cm/s
Cross-shore currents (Site C)	0.322	4.68 cm/s
Along-shore currents (Site D)	0.662	11.24 cm/s
Cross-shore currents (Site D)	0.171	6.38 cm/s
Along-shore currents (Site B)	0.374	4.67 cm/s
Cross-shore currents (Site B)	0.353	3.58 cm/s
Temperature	0.799	1.65ºC
Temperature (adjusted)	0.975	0.52ºC

Table 3a: Correlation coefficients (r-values) for retention resulting from linear regression between the percentage settlement in each area of windward coastal waters and potentially correlated physical variables. Higher values indicate greater correlation. The highest value greater than 0.5 in each column is highlighted in blue. Included environmental variables are: along and cross shore winds averaged over the model run, 10 day along and cross shore wind averages, depth integrated along and cross shore currents (upper 3 m) across the mouth of Kāneʻohe Bay (time averaged), depth integrated along and cross shore currents (below 3 m) across the mouth of Kāneʻohe Bay (time averaged), time averaged flux of water out of Kāneʻohe Bay, time averaged flux of water out of the Inner Bay, time averaged sea surface height (SSH) gradient in the along and cross-shore direction across the mouth of the Inner Bay, time averaged angle of the SSH gradient across the mouth of the Inner Bay, total stream flow for each model run, number of significant rain events during each run (defined by periods with multiple streams exceeding 6 m^3/s flow rates), and Kāneʻohe bay depth integrated salinity (upper 3m) averaged over the model domain and model duration.

Retention Correlation

	Overall	North Coast	Mid Coast	Reef Flat	North Bay	Mid Bay	South Bay	Inner Bay	Mokapu	South Coast
Along-Shore Wind	-0.54	0.32	-0.42	-0.2	-0.61	-0.71	-0.33	0.05	-0.18	-0.17
Cross-Shore Wind	-0.44	0.42	-0.37	-0.18	-0.55	-0.6	-0.24	0.12	-0.13	-0.3
10d Along-Shore Wind	-0.44	0.18	-0.37	-0.14	-0.54	-0.61	-0.23	0.08	-0.05	-0.31
10d Cross-Shore Wind	-0.62	0.29	-0.47	-0.36	-0.58	-0.63	-0.37	-0.18	-0.26	-0.51
3m+ Along Shore Currents	-0.38	0.16	-0.16	0.17	-0.37	-0.58	-0.34	-0.26	0.07	-0.15
3m+ Cross Shore Currents	-0.5	0.45	-0.33	-0.47	-0.42	-0.42	-0.33	-0.02	-0.34	-0.42
3m- Along-Shore Currents	0.31	-0.26	0.34	0.25	0.44	0.37	0.11	-0.18	0.38	0.09
3m- Cross-Shore Currents	0.49	-0.27	0.39	0.13	0.57	0.6	0.38	-0.01	0.17	0.23
Flux out of Bay	0	0.28	-0.06	-0.33	0.08	0.12	0.03	0.18	-0.13	0.04
Flux out of Inner Bay	-0.22	-0.09	0.1	0.34	-0.1	-0.3	-0.41	-0.5	0.19	-0.15
Along-Shore SSH Gradient	0.7	-0.33	0.28	0.26	0.49	0.7	0.67	0.41	0.24	0.32
Cross-Shore SSH Gradient	0.58	-0.41	0.45	0.24	0.63	0.7	0.34	0	0.24	0.4
SSH Gradient Angle	0.58	-0.2	0.04	0.31	0.11	0.36	0.74	0.71	0.24	0.13
Total Stream Flow	-0.12	-0.06	0.01	-0.21	-0.1	-0.02	-0.18	0.01	-0.08	0.21
# Rain Events	-0.35	-0.08	-0.13	-0.3	-0.3	-0.24	-0.34	-0.13	-0.11	0.01
Salinity	0.13	0.1	-0.23	-0.05	-0.1	0.03	0.4	0.34	-0.1	0.16

Table 3b: Correlation coefficients (r-values) for settlement resulting from linear regression between the percentage retention of particles released from each area of windward coastal waters and potentially correlated physical variables. Higher values indicate greater correlation. The highest value greater than 0.5 in each column is highlighted in blue. Included environmental variables are: along and cross shore winds averaged over the model run, 10 day along and cross shore wind averages, depth integrated along and cross shore currents (upper 3 m) across the mouth of Kāneʻohe Bay (time averaged), depth integrated along and cross shore currents (below 3 m) across the mouth of Kāneʻohe Bay (time averaged), time averaged flux of water out of Kāneʻohe Bay, time averaged flux of water out of the Inner Bay, time averaged sea surface height (SSH) gradient in the along and cross-shore direction across the mouth of the Inner Bay, time averaged angle of the SSH gradient across the mouth of the Inner Bay, total stream flow for each model run, number of significant rain events during each run (defined by periods with multiple streams exceeding 6 m^3/s flow rates), and Kāneʻohe bay depth integrated salinity (upper 3m) averaged over the model domain and model duration.

	Settlement Correlation									
	Overall	North Coast	Mid Coast	Reef Flat	North Bay	Mid Bay	South Bay	Inner Bay	Mokapu	South Coast
Along-Shore Wind	-0.54	-0.01	0.2	-0.14	-0.7	0.12	-0.46	-0.17	0.16	0.2
Cross-Shore Wind	-0.44	-0.01	0.22	-0.2	-0.58	0.15	-0.57	-0.08	0.22	0.26
10d Along-Shore Wind	-0.44	-0.13	0.09	-0.08	-0.39	-0.14	-0.11	-0.28	0.11	0.12
10d Cross-Shore Wind	-0.62	-0.05	0.09	-0.3	-0.33	-0.33	-0.28	-0.4	-0.03	-0.08
3m+ Along Shore Currents	-0.38	0.02	0.21	-0.03	-0.34	0.19	0.03	-0.37	0.12	0.15
3m+ Cross Shore Currents	-0.5	-0.11	-0.12	-0.25	-0.48	-0.12	-0.52	-0.14	0.21	0.36
3m- Along-Shore Currents	0.31	-0.33	-0.34	0.24	0.26	0.29	0.42	0.09	-0.12	-0.11
3m- Cross-Shore Currents	0.49	-0.2	-0.3	0.04	0.57	-0.08	0.4	0.25	-0.2	-0.29
Flux out of Bay	0	-0.18	-0.16	-0.11	-0.12	0.12	-0.37	0.2	0.02	0.19
Flux out of Inner Bay	-0.22	0.12	0.17	0.19	0.07	0.1	0.52	-0.6	0.09	0.12
Along-Shore SSH Gradient	0.7	0.08	0	0.07	0.58	0.01	0.09	0.57	-0.26	-0.39
Cross-Shore SSH Gradient	0.58	0.02	-0.15	0.23	0.64	-0.07	0.5	0.22	-0.22	-0.28
SSH Gradient Angle	0.58	0.13	0.23	0.03	0.17	0.16	-0.2	0.72	-0.14	-0.47
Total Stream Flow	-0.12	0.15	-0.04	0.13	-0.05	-0.13	-0.08	-0.13	0.21	0.12
# Rain Events	-0.35	0.18	-0.02	0.15	-0.26	-0.14	-0.12	-0.3	0.33	0.12
Salinity	0.13	0	0.16	-0.39	-0.02	-0.12	-0.49	0.44	-0.08	-0.07

FIGURES

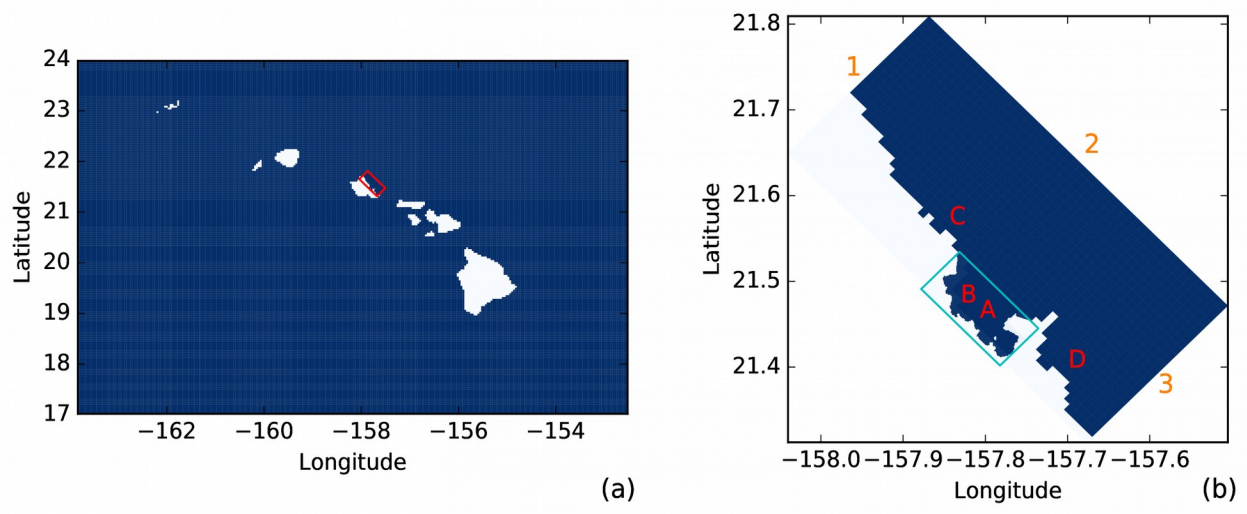

Figure 1: (a) Study area (1 km Oʻahu windward coast grid, outlined in red) inset within the Hawaiian Islands 4 km ROMS grid. (b) 1 km Oʻahu windward coast grid with 0.1 km Kāneʻohe Bay grid inset (outlined in blue). Instrument deployment sites are labeled A,B,C,D. Northwest, Northeast, and Southeast grid boundaries are labeled 1,2,3.

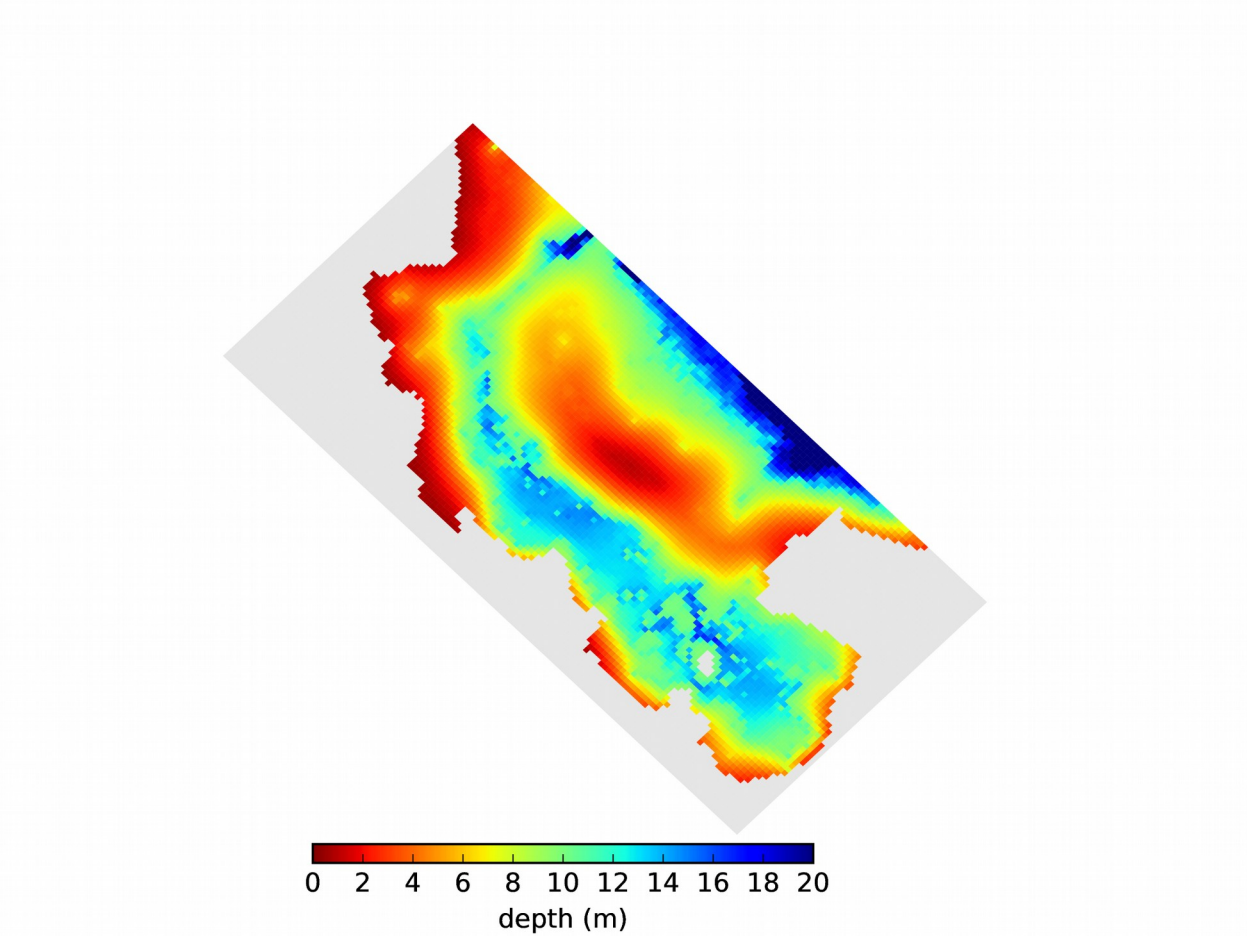

Figure 2: Kāneʻohe Bay bathymetry at 100 m resolution (from the Kāneʻohe Bay model grid). Red areas are shallower, blue areas are deeper. The large barrier reef and fringing reefs (red/orange) along with the lagoon and northern channel (light-dark blue) can be readily identified.

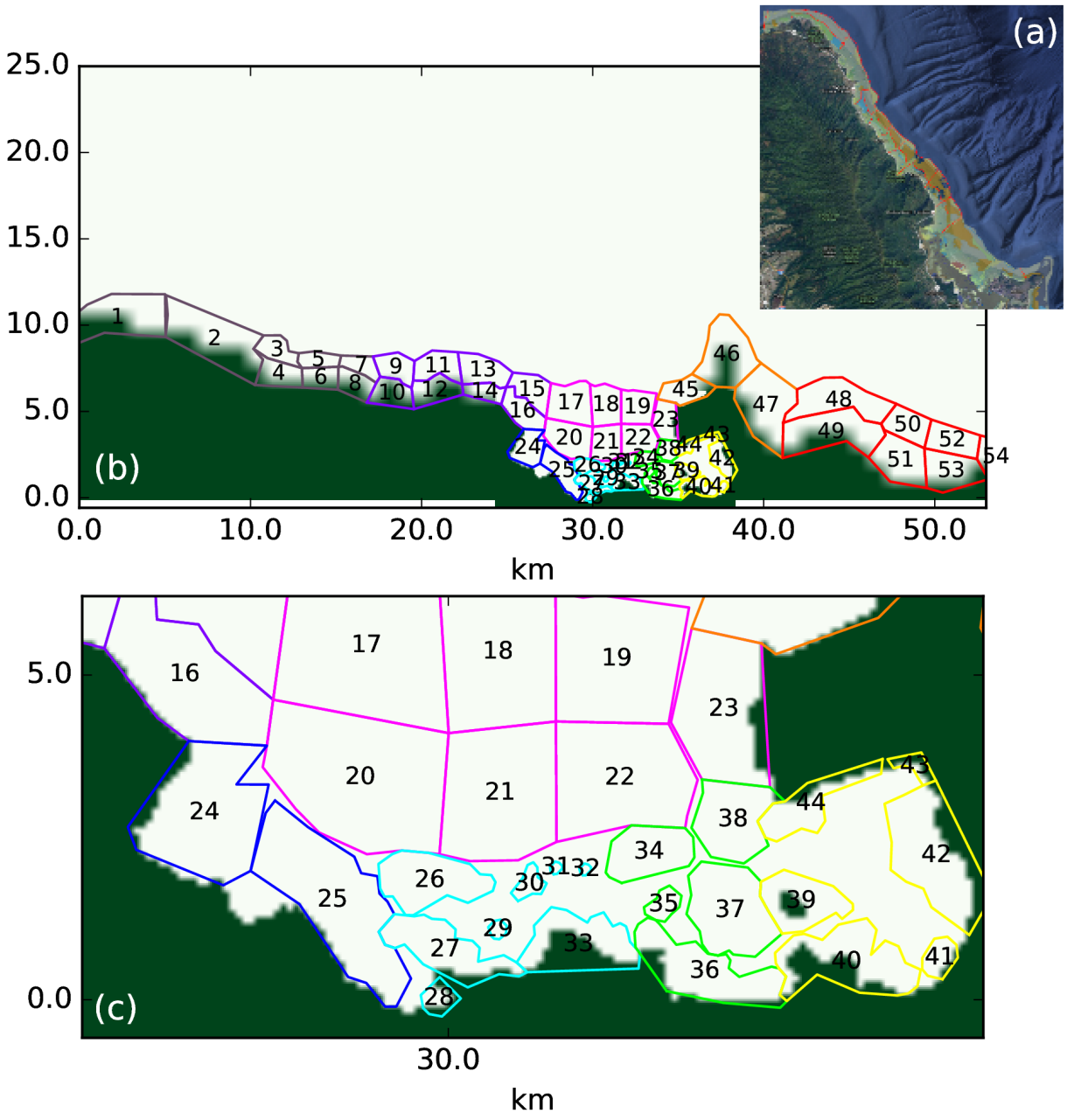

Figure 3: (a) NOAA NCCOS shallow water benthic habitat map for windward Oʻahu with sample divisions drawn based off of topography. Habitat polygons (source/sink sites) for windward coast (b) and Kāneʻohe Bay (c). Colored by area: North Coast (1-8), Mid Coast (9-14), Reef Flat (17-23), North Bay (24-25), Mid Bay (26-33), South Bay (34-38), Inner Bay (39-44), Mokapu (45-47), South Coast (48-54).

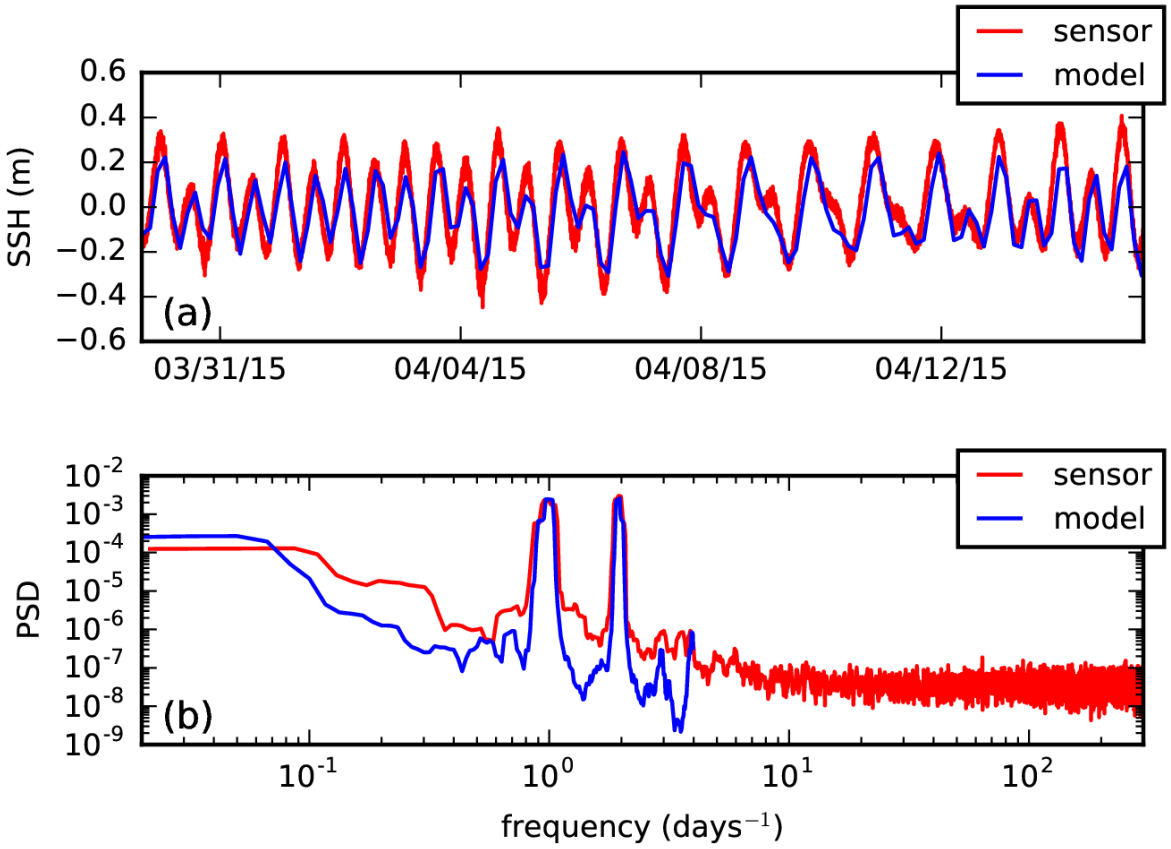

Figure 4: (a) Time series comparison of observed (red) and modeled (blue) SSH at site C. (b) Spectrum of observed and modeled and modeled SSH data at Site C.

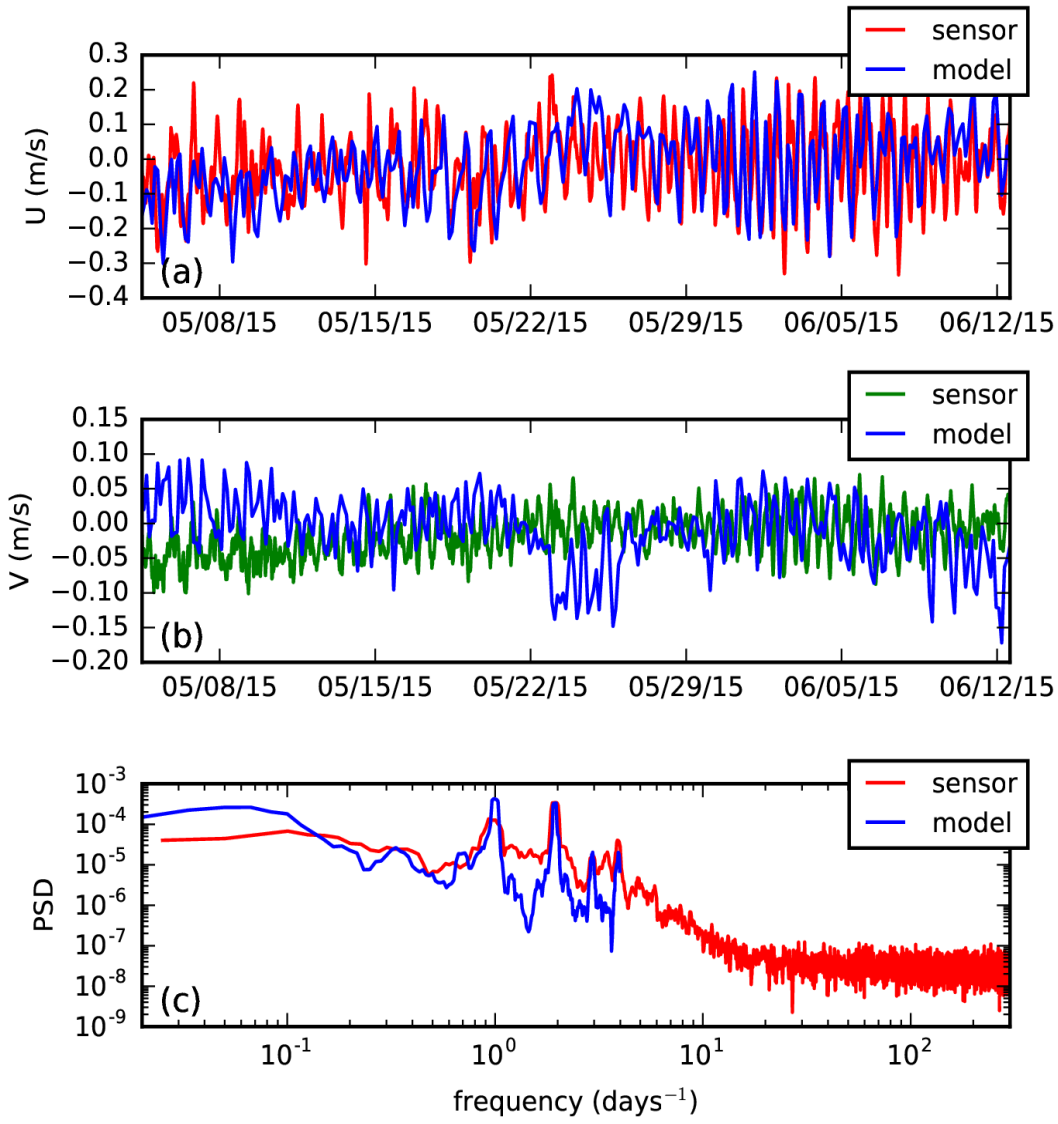

Figure 5: Time series of observed and modeled along-shore (a) and cross-shore (b) 3 hr. depth integrated currents at site C. Rotary current spectrum (c) of observed and modeled depth-integrated currents at site D.

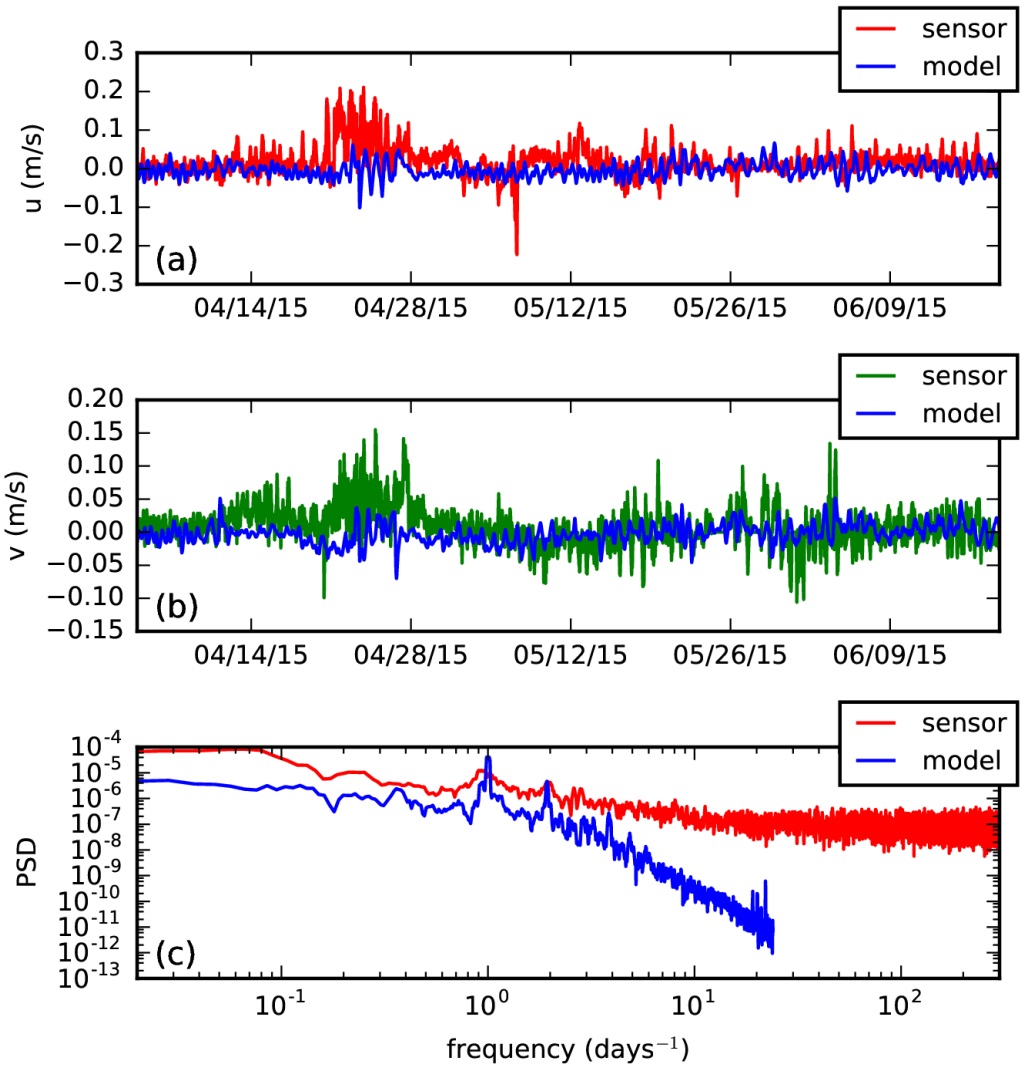

Figure 6: Time series of observed and modeled along-shore (a) and cross-shore (b) 30 min currents at site B. Rotary current spectrum (c) of observed and modeled currents at site B.

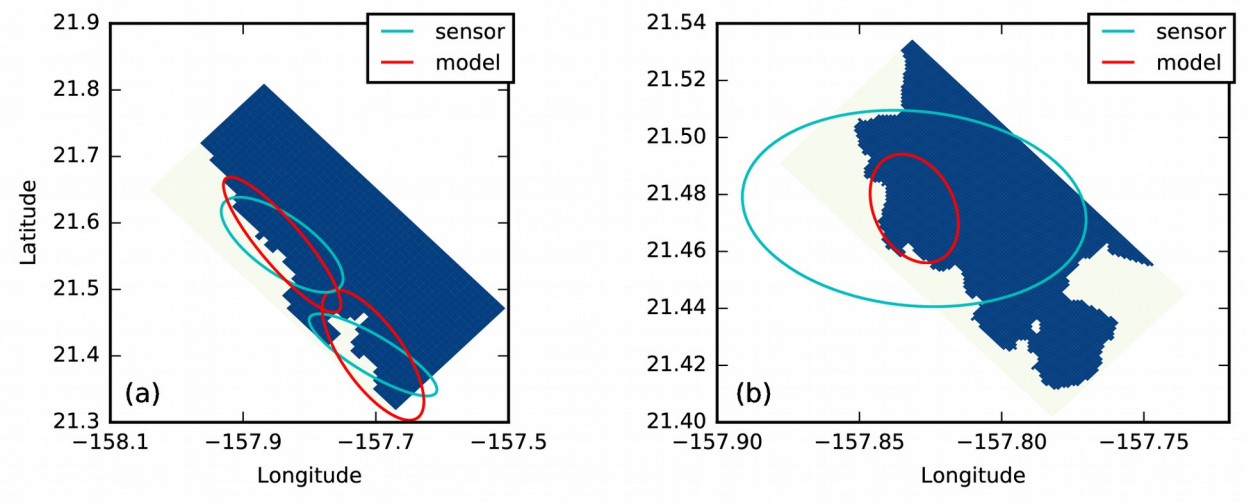

Figure 7: (a) Current ellipse comparison between ADP measurements (blue) and windward coast ROMS model (red) at sites C and D. (b) Current ellipse comparison between current meter measurements (blue) and Kāneʻohe Bay ROMS model (red) at site B.

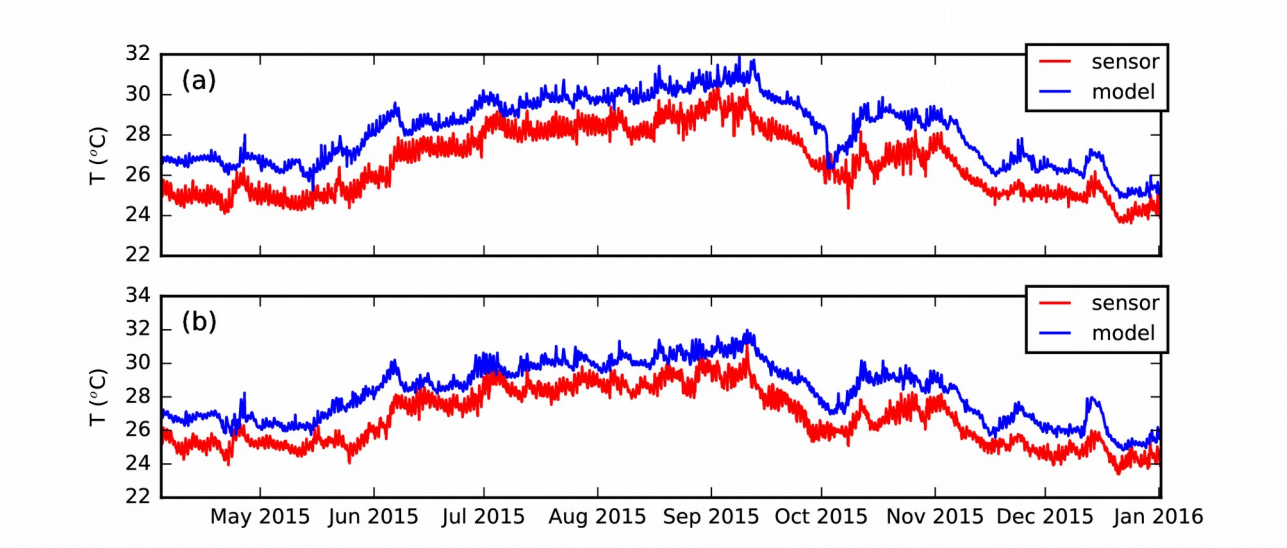

Figure 8: Time series of observed and modeled 1 m temperature at site A (a) and site B (b).

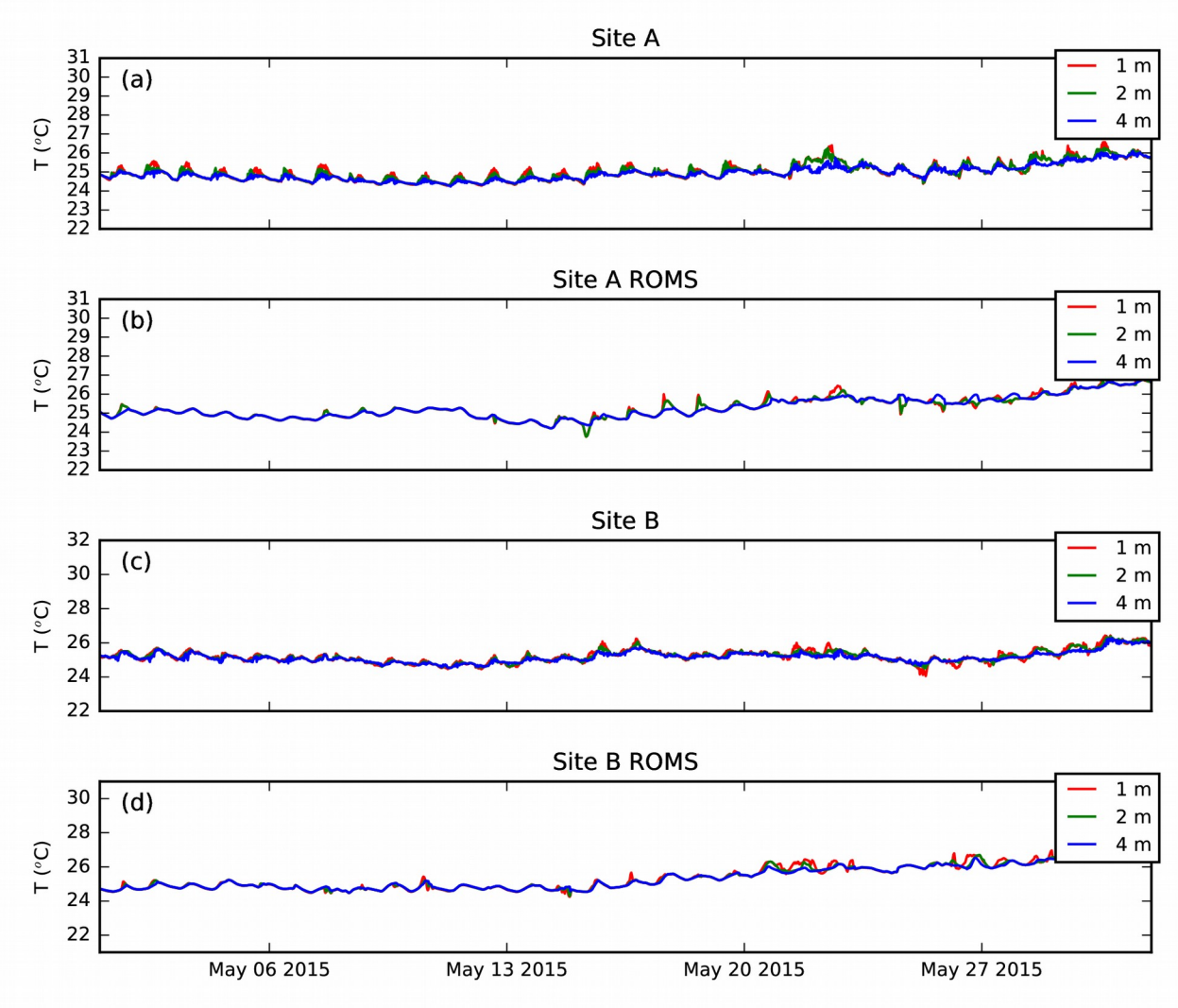

Figure 9: 10 day time-series of temperature at 1 m, 2 m, and 4 m at Sites A and B within Kāneʻohe Bay to depict daily variability. Plots (a) and (b) depict observed and modeled temperatures at Site A. Plots (c) and (d) depict observed and modeled temperatures at Site B.

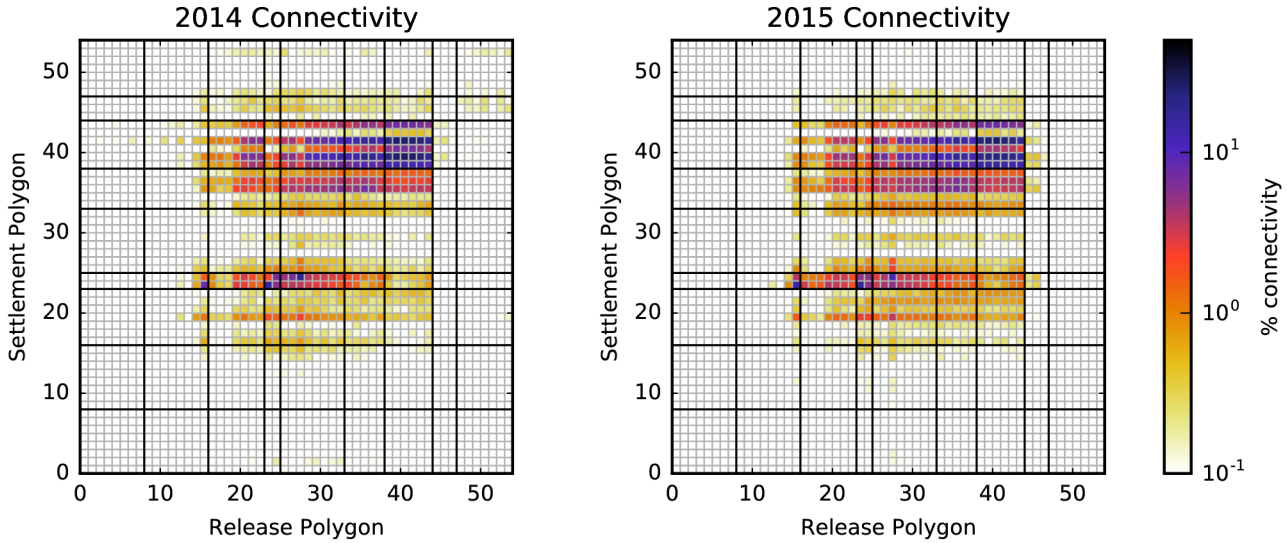

Figure 10: Connectivity grids for 2014 and 2015. Rows and columns represent individual polygons (as numbered in Figure 2b,c). The grid cell at the intersection of each row and column displays the percentage of particles released from the column polygon that settled in the row polygon. Values are displayed on a logarithmic scale. The dark gridlines are used to section the grid into the areas described in Methods and in Figure 2.

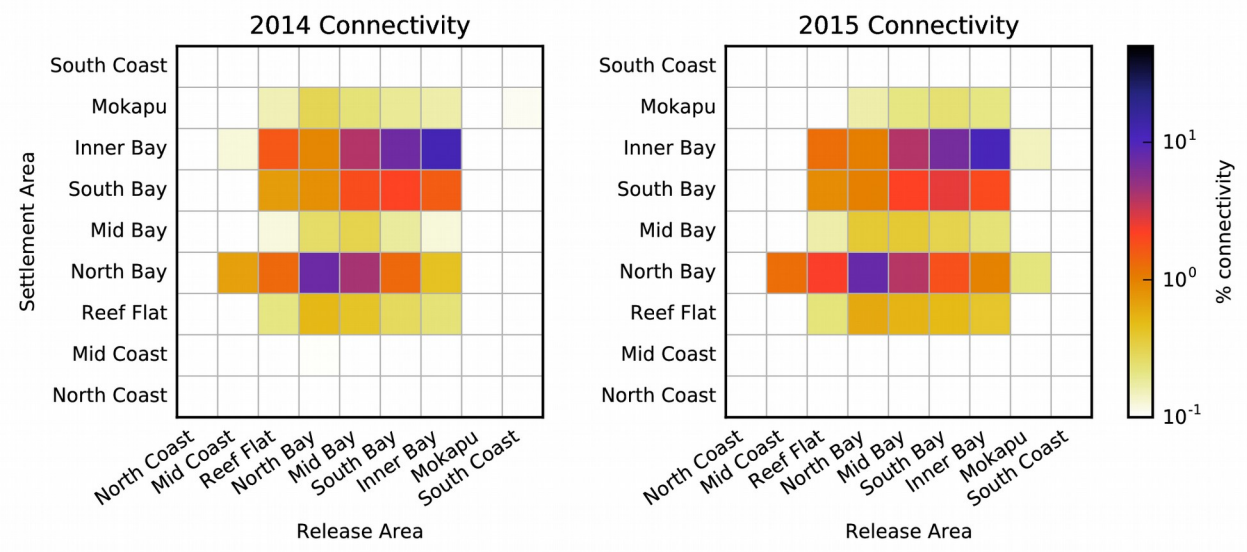

Figure 11: Connectivity grids for 2014 and 2015 displaying percentage connectivity between areas. Scale is logarithmic.

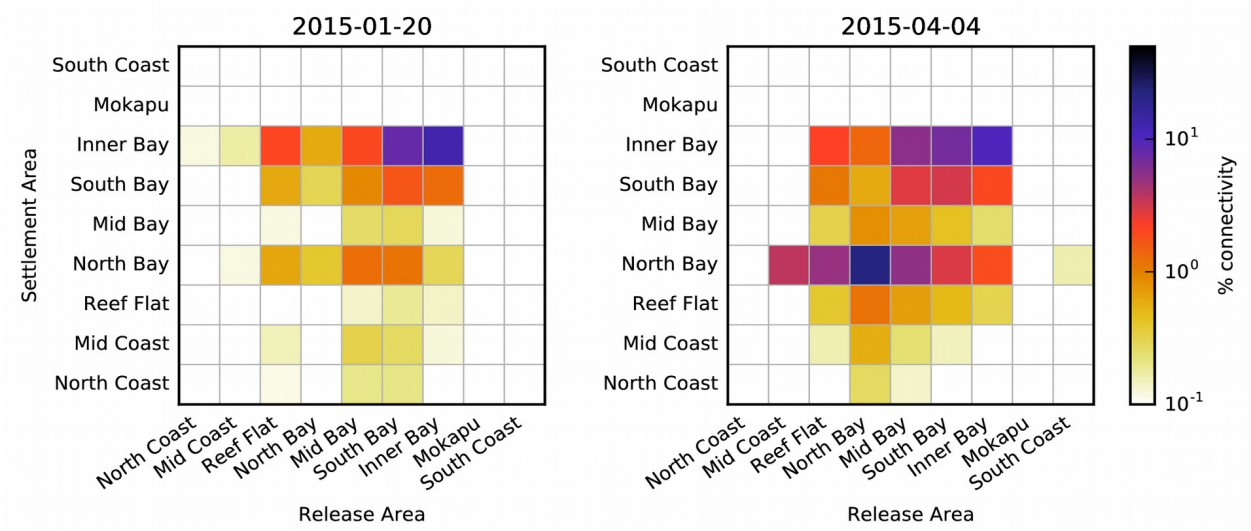

Figure 12: Connectivity grids for Jan 20, 2015 and April 4, 2015 displaying percentage connectivity between areas. Scale is logarithmic.

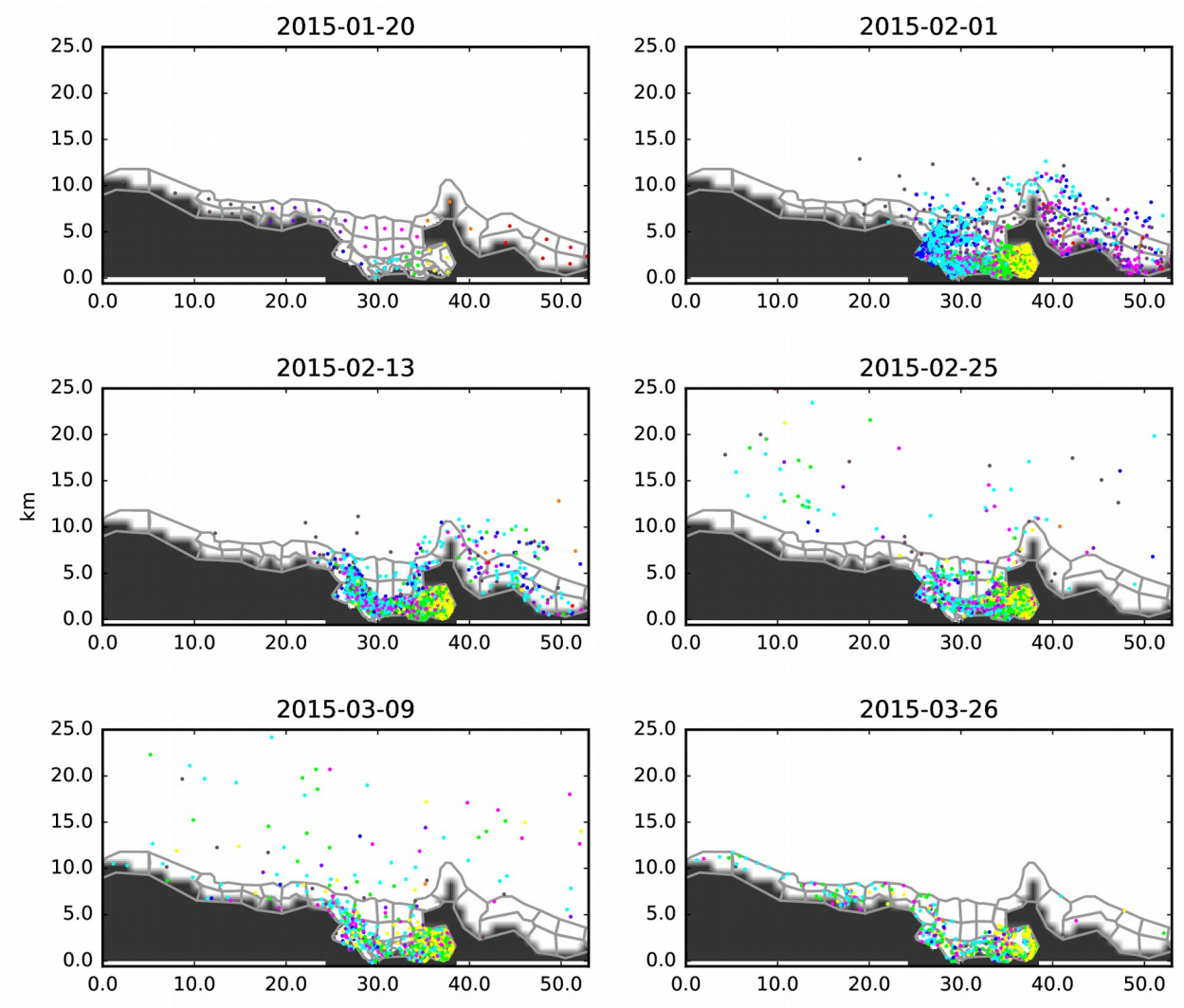

Figure 13a: Particle dispersion for January 20, 2015 simulation. Particle colors are coded by release area.

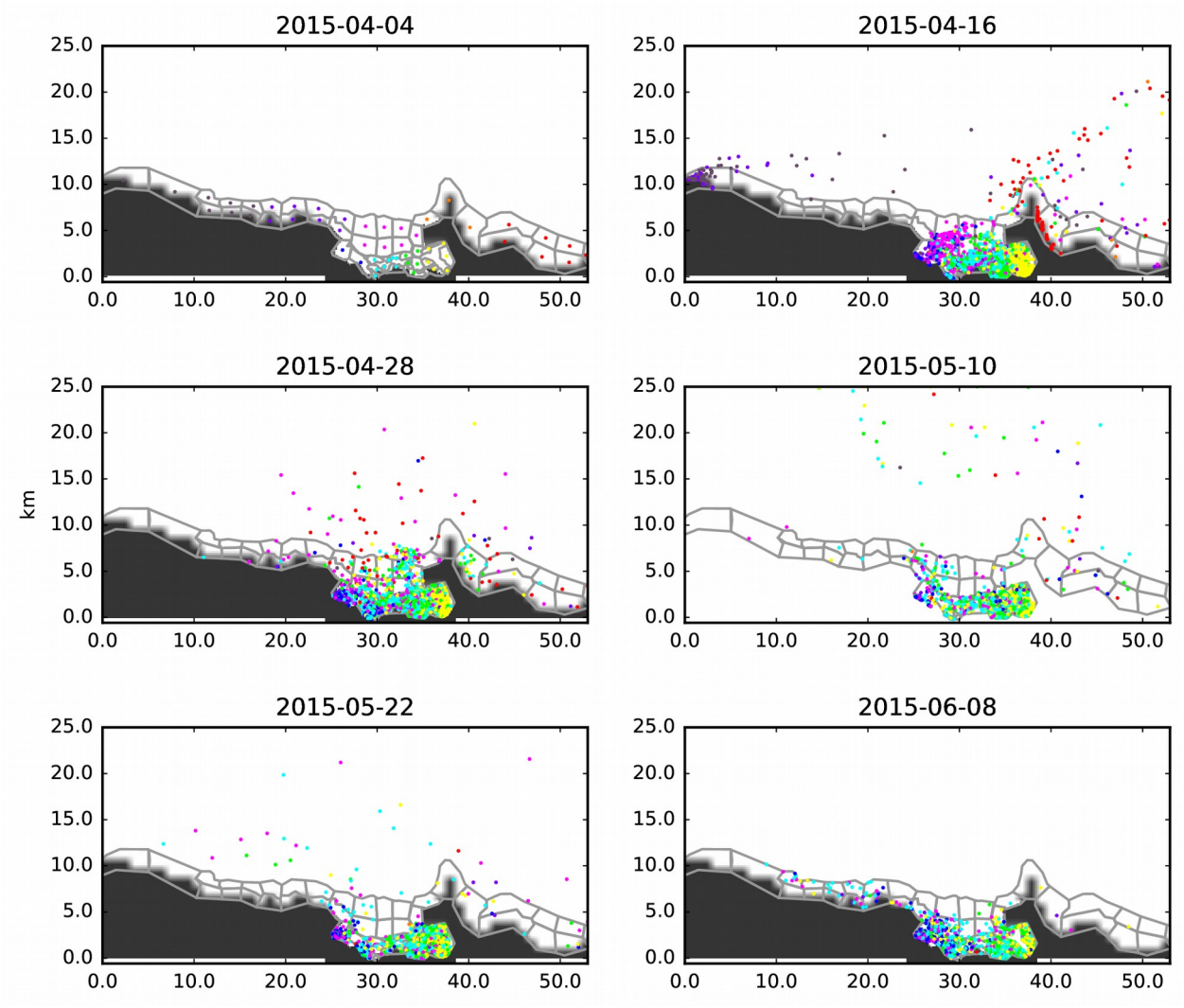

Figure 13b: Particle dispersion for April 4, 2015 simulation. Particle colors are coded by release area.

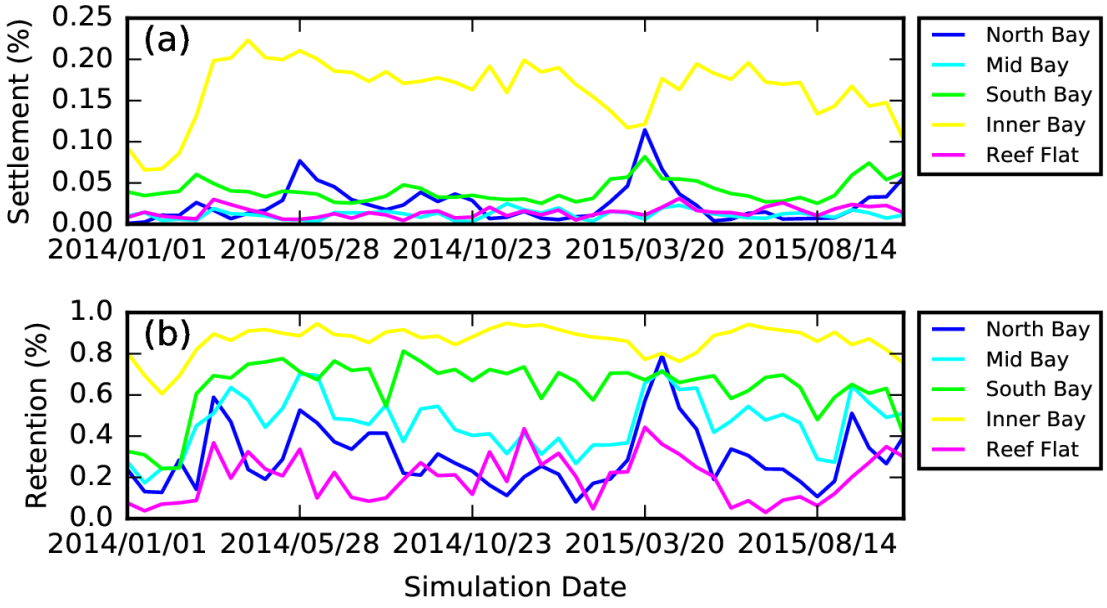

Figure 14: Settlement (a) and retention (b) plotted as time series for different sections of Kāneʻohe Bay. Settlement is percentage of total number of particles released that settled in that area. Retention is percentage of particles released from that area that settled in some area.

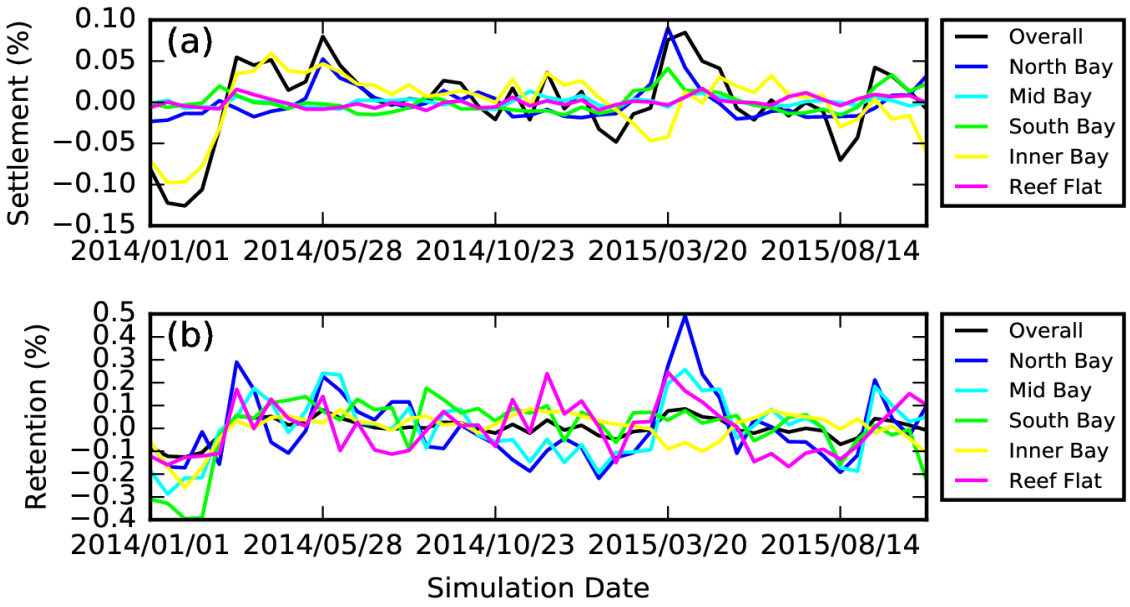

Figure 15: Settlement (a) and retention (b) plotted as time series (with the mean removed from each series) for different sections of Kāneʻohe Bay. Settlement is percentage of total number of particles released that settled in that area. Retention is percentage of particles released from that area that settled in some area.

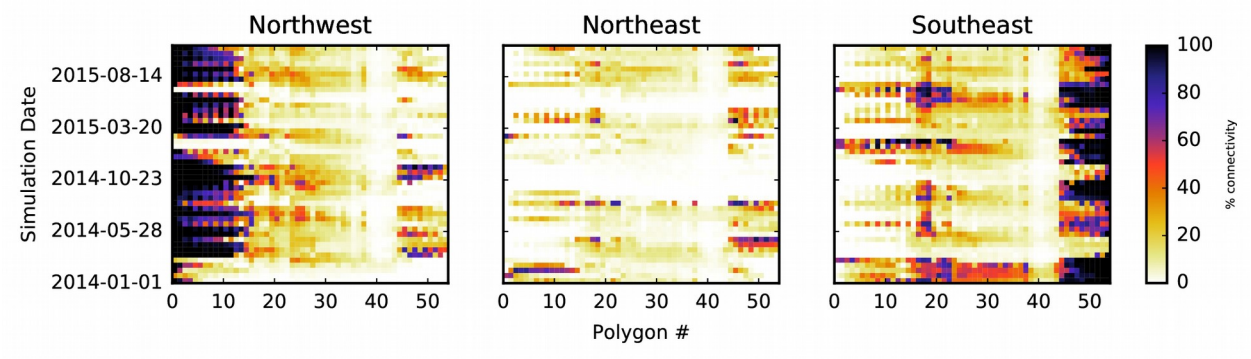

Figure 16: Depiction of particle loss through Northwest, Northeast, and Southeast grid boundaries. Each column represents a different polygon/release point. Each row represents a different simulation starting with Jan 1, 2014 simulation (bottom row). Cell value is percentage of particles from that release point passing through the boundary.

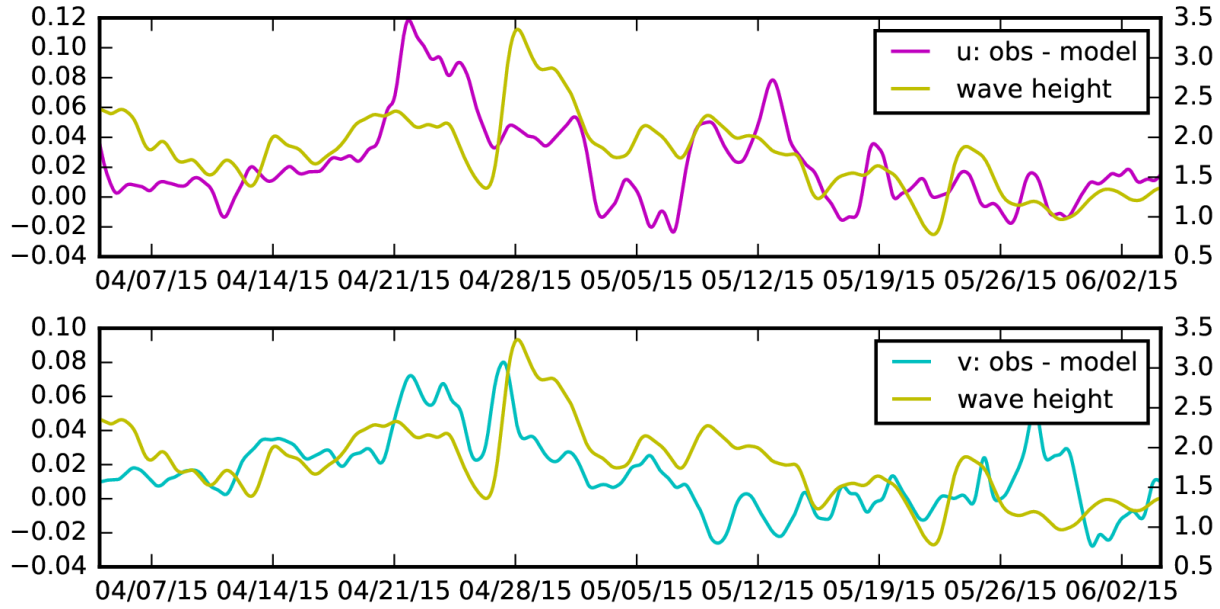

Figure 17: Time series of difference between observed and modeled along-shore (u) and cross-shore (v) currents at Site B location within Kāneʻohe Bay compared with wave heights as measured just outside of Kāneʻohe Bay. Series were smoothed with a 24 hr. filter.

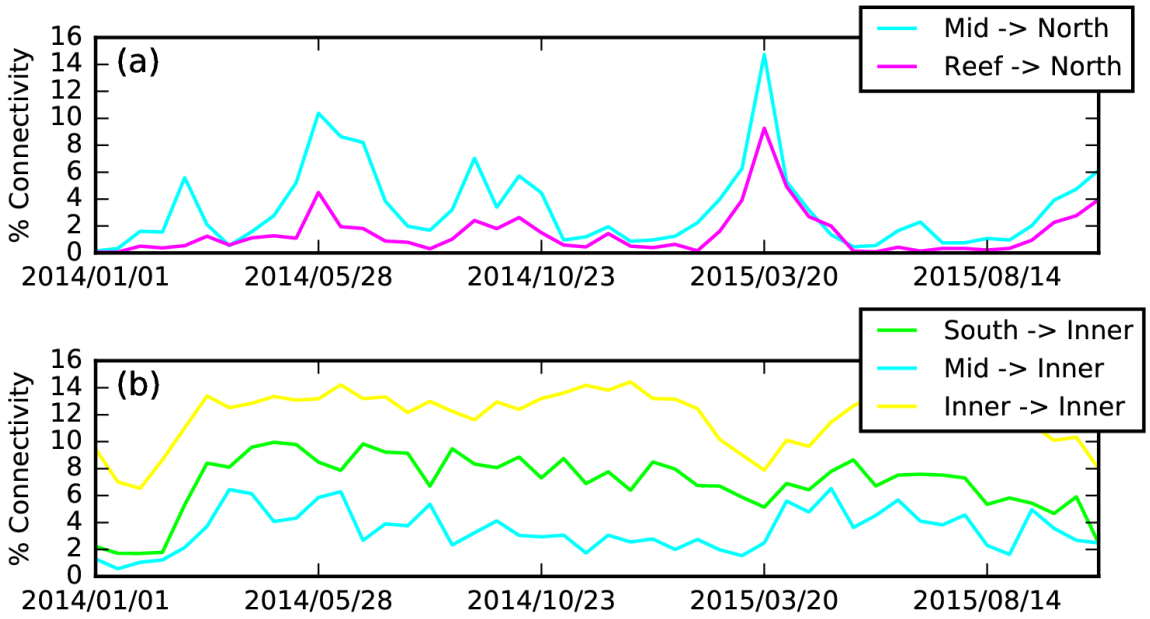

Figure 18: (a) Timeseries of Mid Bay and Reef Flat to North Bay connectivity (as percentage of particles released from Mid Bay and Reef Flat areas that settled in the North Bay area). (b) Timeseries of South, Mid and Inner Bay to Inner Bay connectivity (as percentage of particles released from the South, Mid and Inner Bay areas that settled in the Inner Bay area).

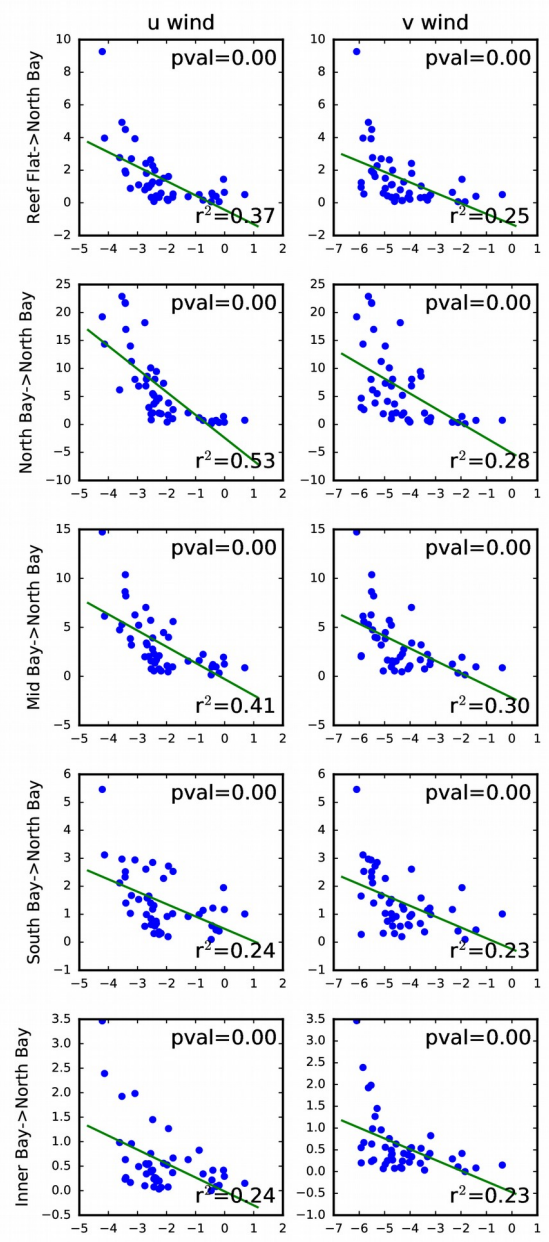

Figure 19: Along-shore (u wind) and cross-shore (v wind) wind velocities for each simulation (time and spatially averaged) plotted against connectivity between each area of the bay and the North Bay (percentage of particles released from an area that settled in the North Bay). For each plot, the regression line is displayed in green, and the p-value and r^2 values from the regression are displayed in the upper and lower right corners respectively.

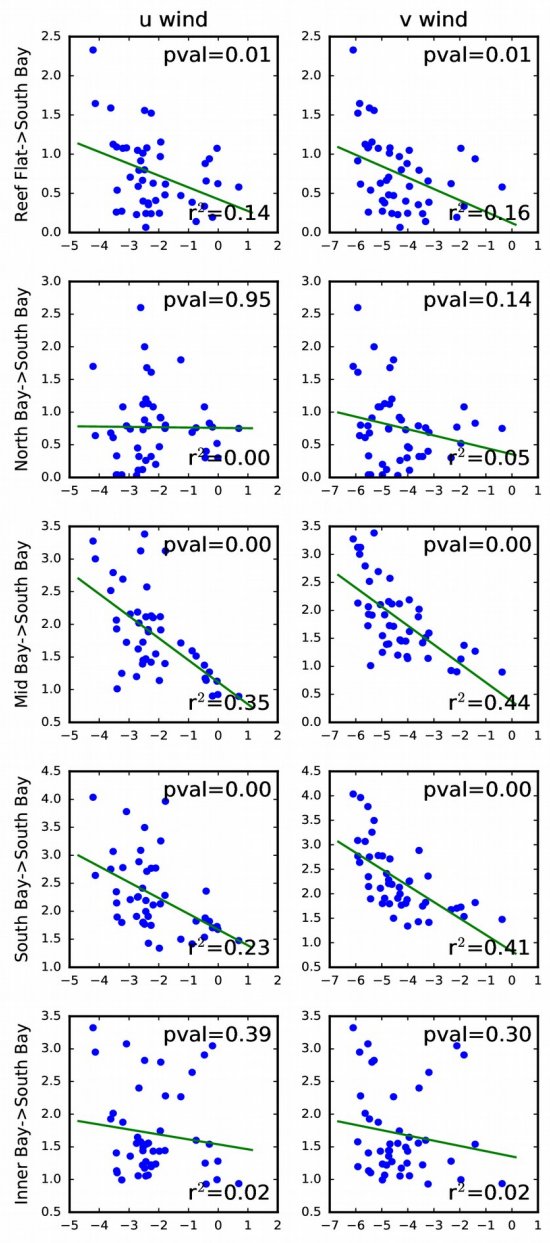

Figure 20: Along-shore (u wind) and cross-shore (v wind) wind velocities for each simulation (time and spatially averaged) plotted against connectivity between each area of the bay and the South Bay (percentage of particles released from an area that settled in the South Bay). For each plot, the regression line is displayed in green, and the p-value and r^2 values from the regression are displayed in the upper and lower right corners respectively.

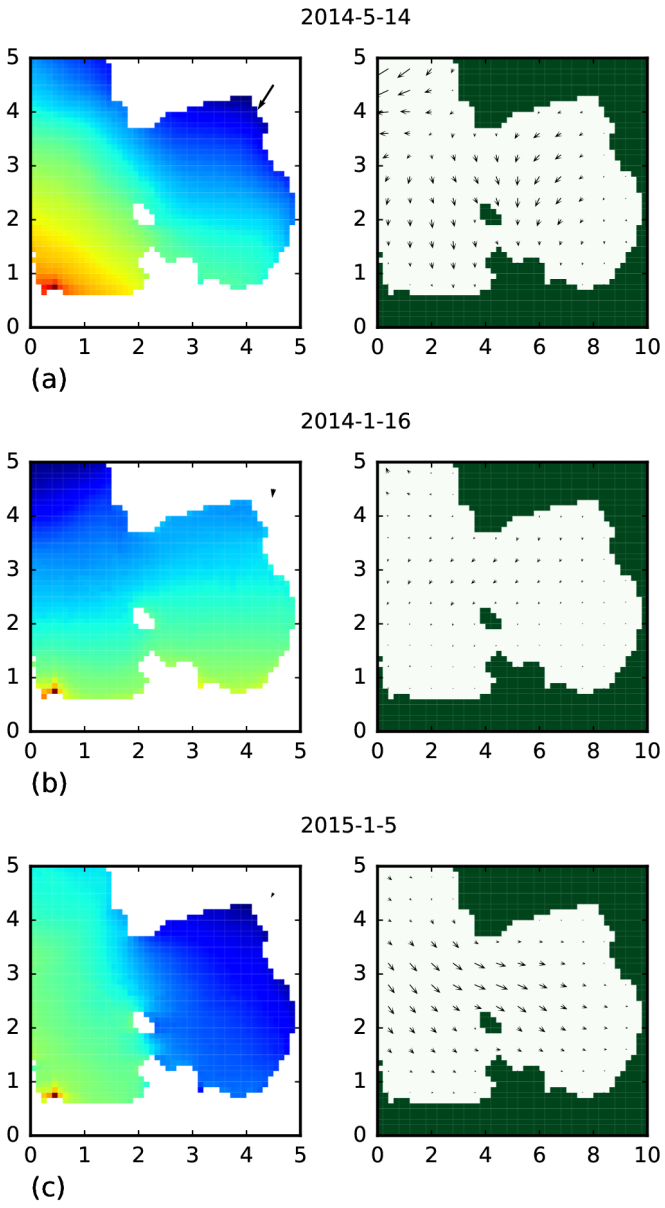

Figure 21: 55 day time averaged SSH for the South Bay and Inner Bay areas along with 3m depth integrated surface currents for Kāneʻohe Bay. Typical gradient angle and current patterns displayed in (a). "Open" gradient displayed in (b), along with surface currents directed out of the Inner Bay. "Closed" gradient displayed in (c) with surface currents directed into the Inner Bay.

APPENDIX A

Particle Tracking Model Comparison

Three particle tracking models were considered for use in this project: TracPy (Thyng and Hetland 2014), the Lagrangian Transport model (LTRANS) (North et al. 2011) and the Connectivity Modeling System (CMS) (Paris et al. 2013). All three operate as offline lagrangian particle tracking models, that is, they utilize current velocity fields previously generated by oceanographic models (such as ROMS), to calculate particles trajectories through time throughout the model domain. It is also possible to perform this type of calculation online, i.e., while the oceanographic model is running, in order to make use of the highest resolution fields generated by the model. However, due to the high computational cost of hydrodynamic simulations, running repeated simulations is often not practical, and so necessitates the use of an offline model (Thyng and Hetland 2014).

LTRANS and CMS both operate natively in Fortran. TracPy differs in that it is a Python wrapper for the Fortran based TRACMASS Lagrangian trajectory model. TracPy is designed for use with the Python Notebook, as opposed to the terminal interface required by LTRANS and CMS. A comparison of characteristics of the three models is given in Table A1. For the Speed and Ease of Use categories, the models were ranked in order from 1 to 3, with 1 indicating most favorable and 3 indicating least favorable. For the ease of use category, it should be noted that this is a subjective assessment and is specifically in regard to the operation of each trajectory model with ROMS output.

The decision was ultimately made to utilize the CMS model, despite the compatibility issues with ROMS, primarily for the ability of this model to work with nested grids. This function was necessary to allow the use of both the high-resolution Kāneʻohe Bay model with the lower resolution windward coast model during the simulations. The biological parameterizations available within CMS and the ability of the model to perform hindcasts were also considered during this selection.

A number of test simulations were performed using identical parameters for both the CMS and LTRANS models, primarily to verify that CMS was moving particles correctly following the manipulation of the ROMS output data to fit the CMS input requirements (Figure A1). This process proved valuable in identifying specific quirks in CMS, such as the (undocumented) requirement that vertical velocities be positive downward.

Table A1: Overview/comparison of the TracPy, LTRANS and CMS particle tracking models

	TracPy	**LTRANS**	**CMS**
Speed	3	2	1
Ease of Use	1	2	3
Can work directly with ROMS output	Yes	Yes	No
Reverse Tracking	Yes	No	Yes
Ability to work with nested grids	No	No	Yes
Biological Parameterizations	No	Yes	Yes

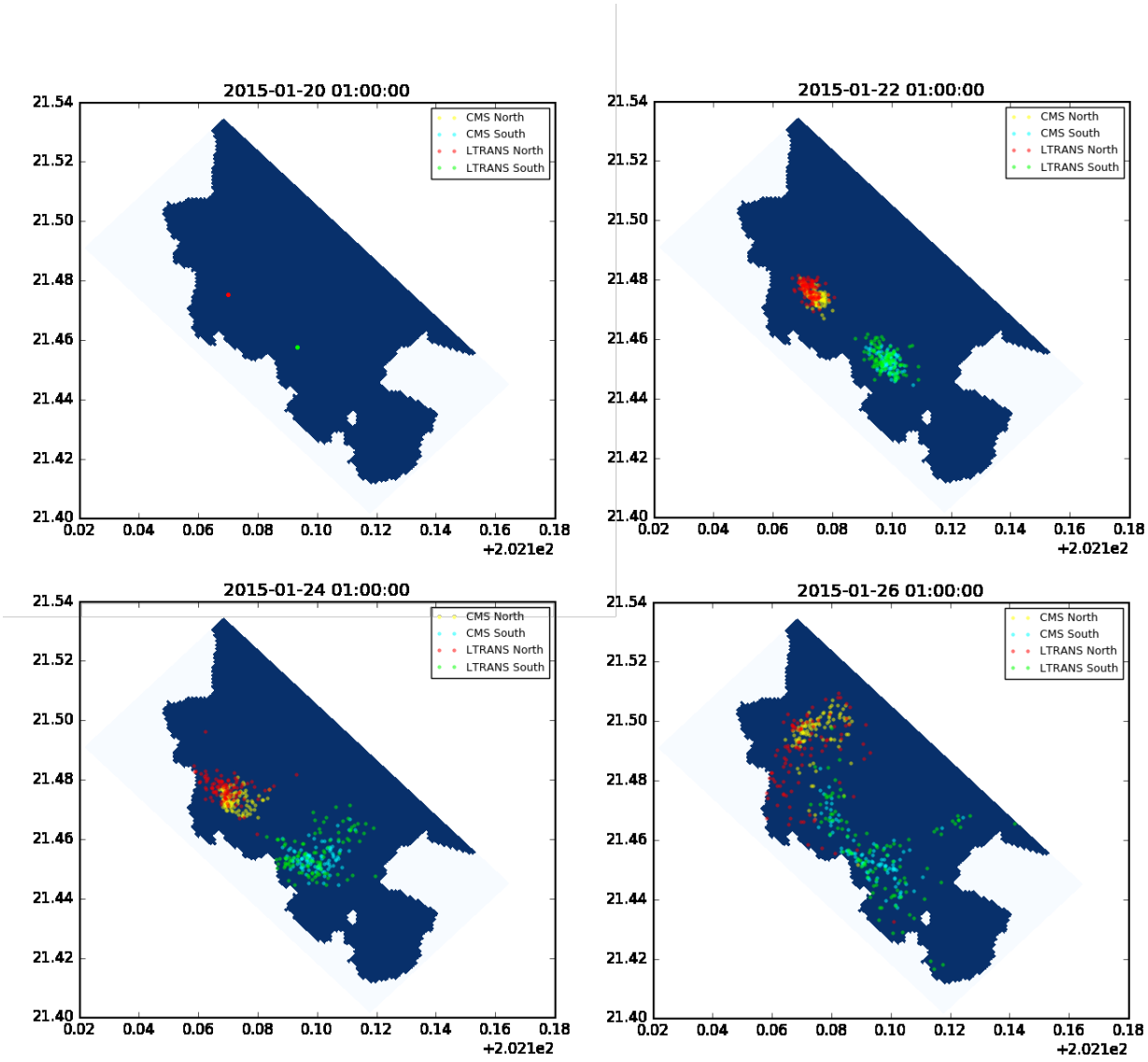

Figure A1: Comparison of particle advection/dispersion within Kāneʻohe Bay over a 6 day period as generated by the CMS and LTRANS particle tracking models.

APPENDIX B

Analysis of temperature data

The following is an analysis of the data collected by the 6 SBE39 thermistors deployed in Kāneʻohe Bay from April 3, 2015 to April 5, 2016. The sensors were located on two patch reefs located ~5 km apart in the lagoon area of the bay. Three thermistors were deployed on each patch reef at 1 m, 2 m, and 4 m depth. Temperature measurements were made at 2 minute intervals. A pre-deployment test returned a mean sensor error of ~0.04 ^{o}C.

The series appear to exhibit both a strong diurnal signal (daily heating) and a strong annual signal (summer/winter) (Figures B1, B2, B3). Annual variance is ~7 ^{o}C. The mean temperature difference between the 1 m and 4 m is sensors relatively small, 0.1 ^{o}C or less, and is typically exceeded by the daily variability (~1 ^{o}C at 1 m and >0.5 ^{o}C at 4 m). As a result, temperatures at 1 m frequently dip below temperatures at 2 m and 4 m during the coolest part of the daily cycle (4am - 8am HST). There is an extended temperature inversion at the northern site from September 20 - October 5, while temperatures at the southern site are essentially homogenized through the (upper 4 m of the) water column during the same period (Figures B1, B2). The cause of this inversion is unclear; a possible explanation is as a response to an extended weather event.

Spectra show a significant peak at 1 cycle / day (as expected) and in the first harmonic, along with smaller amounts of energy in the second and third harmonics (Figures B4, B5). The northern site spectra also show a small amount of energy at the M2 tidal frequency (perhaps due to proximity to the northern channel), while the southern site exhibits significantly less energy at

that frequency (Figure B5). There is a definite peak in coherence at 1 cycle/day between the two sites at all measured depths, and a peak at 2 c.p.d. at 1 m depth (Figure B6). The phase is a constant 0 at lower frequencies (as expected), but begins to start fluctuating above 10 c.p.d.

There is a very high correlation between the two sites at each depth: 0.982 at 1 m, 0.987 at 2 m, and 0.989 at 4 m. This is likely at least in part a result of the long-term variability. Repeating the correlations after running a high-pass filter to focus on the daily variability results in substantially lower coefficients: 0.216 at 1 m, 0.402 at 2 m, and 0.669 at 4 m. So there is significantly less correlation once long-term trends are removed. One other point of note is that correlation between the two sites increases with increasing depth, which makes sense as both waves and air/sea interactions should result in more variability near the surface.

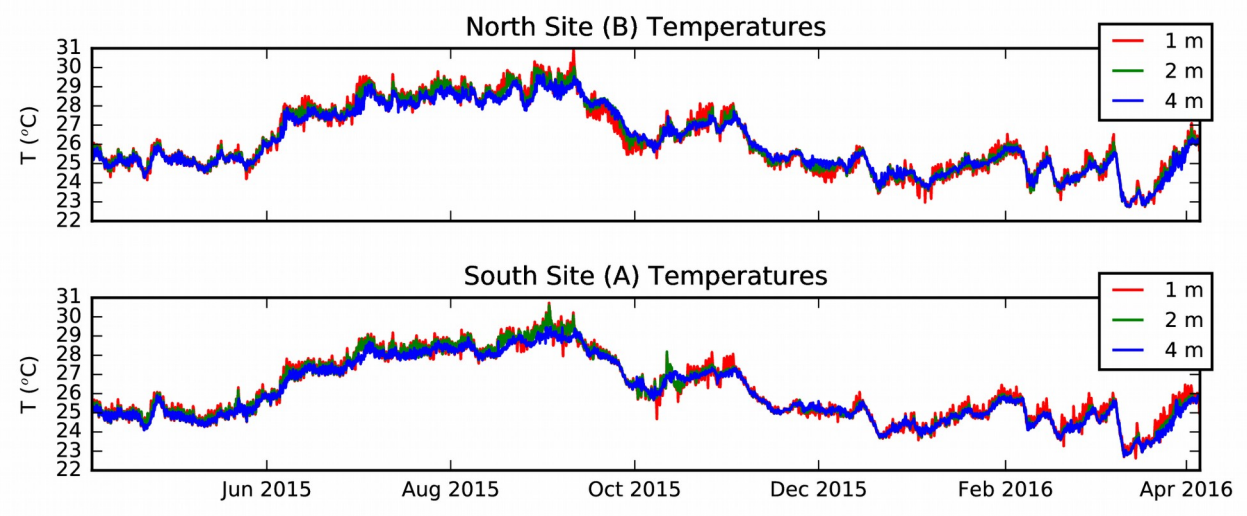

Figure B1: Time-series of observed temperatures at Sites A and B within Kāneʻohe Bay. Temperature measurements were at 1 m, 2 m, and 4 m depth at each site.

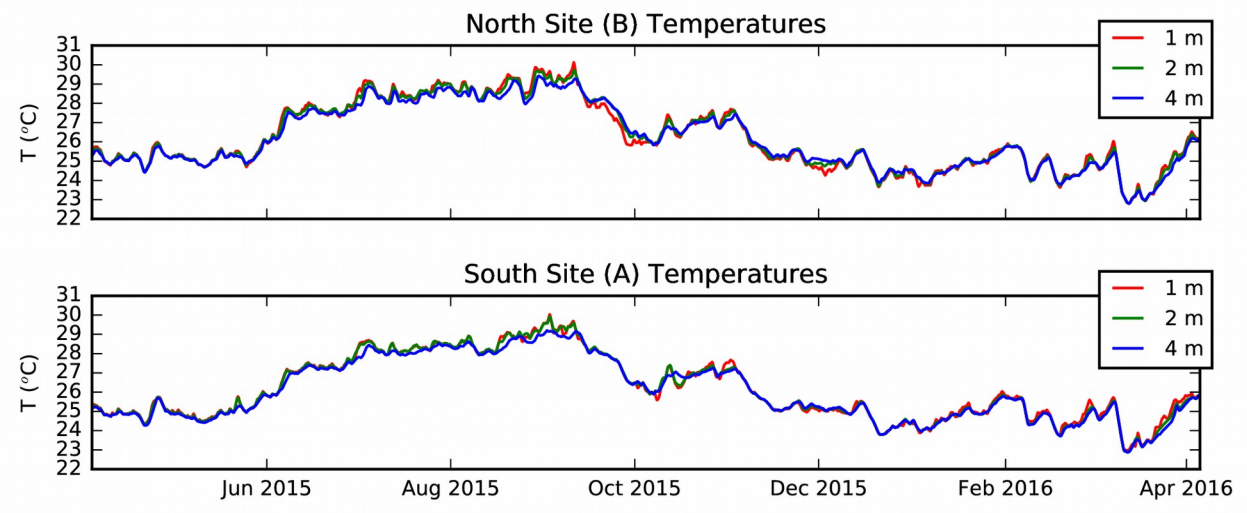

Figure B2: Time-series of daily averaged temperatures at Sites A and B within Kāneʻohe Bay. Temperature measurements were at 1 m, 2 m, and 4 m depth at each site.

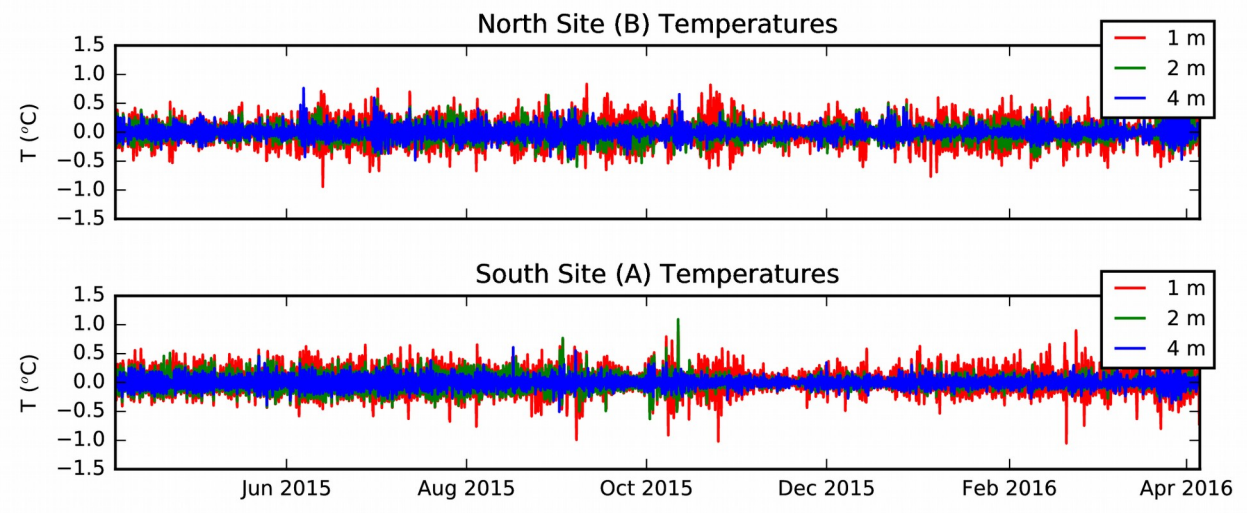

Figure B3: Time-series of temperatures at Sites A and B within Kāneʻohe Bay. A 24 hour highpass filter has been applied to remove long-term variability. Temperature measurements were at 1 m, 2 m, and 4 m depth at each site.

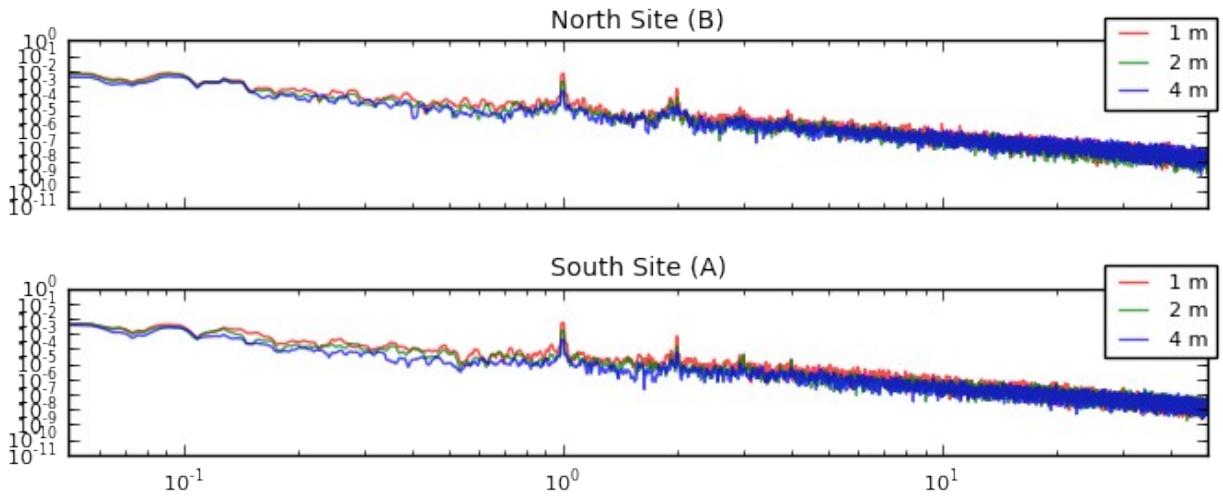

Figure B4: Power spectrum of observed temperatures at Sites A and B within Kāneʻohe Bay. Log-log scale. Temperature measurements were at 1 m, 2 m, and 4 m depth at each site.

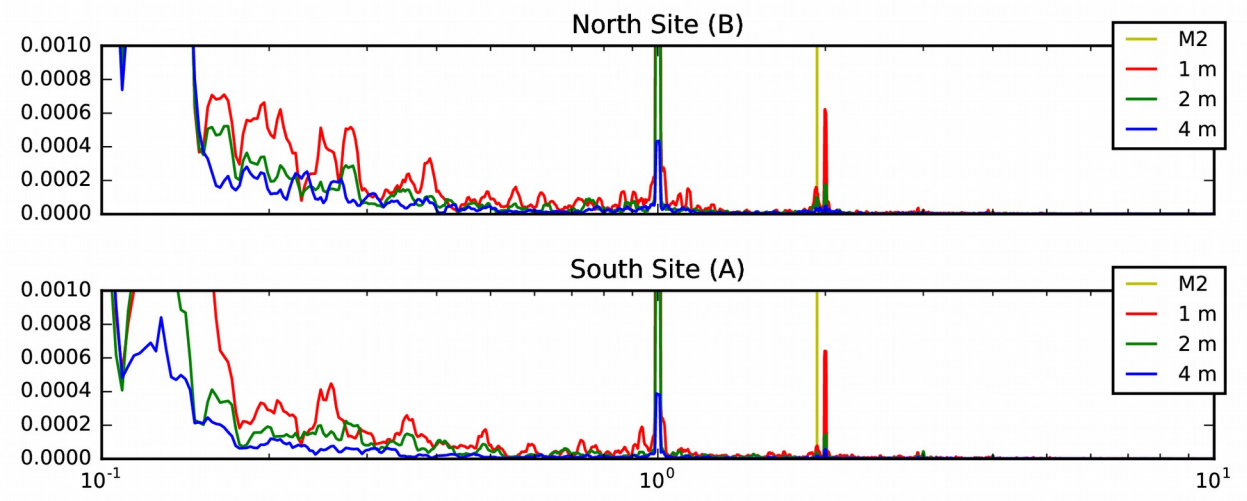

Figure B5: Power spectrum of observed temperatures at Sites A and B within Kāneʻohe Bay. Semi-log scale. Yellow bar denotes M2 tidal frequency. Temperature measurements were at 1 m, 2 m, and 4 m depth at each site.

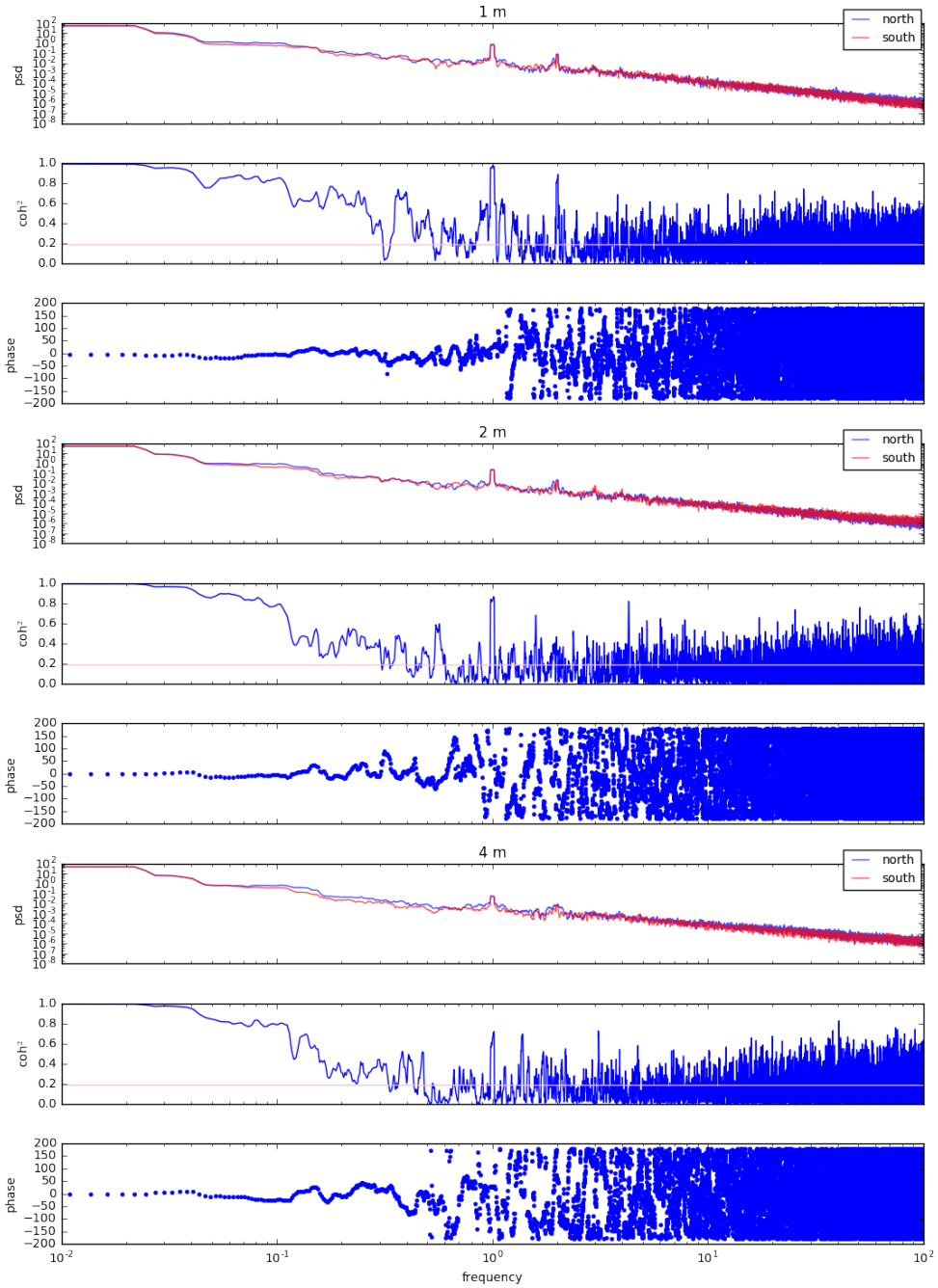

Figure B6: Cross-spectrum, squared coherence, and phase difference between observed temperatures at 1 m, 2 m, and 4 m depth at Sites A and B within Kāneʻohe Bay.

REFERENCES

BAE Systems Sensor Solutions Identification & Surveillance (S2 IS), 2007. Mapping of Benthic Habitats for The Main Eight Hawaiian Islands Task Order I Project Completion Report. Prepared under: NOAA Contract No.: DG133C-02CN-007

Bathen, K.H., 1968. A descriptive study of the physical oceanography of Kaneohe Bay, Oahu, Hawaii. Report no. 14. Honolulu, HI: Hawaii Institute of Marine Biology.

Brothers, E.B. and R.E. Thresher, 1985. Pelagic duration, dispersal, and the distribution of Indo-Pacific coral reef fishes. *The ecology of coral reefs*, *3*(1), pp.53-69.

Cowen, R.K. and S. Sponaugle, 2009. Larval dispersal and marine population connectivity. *Marine Science*, *1*.

Cowen, R.K., C.B. Paris, and A. Srinivasan, 2006. Scaling of connectivity in marine populations. *Science*, *311*(5760), pp.522-527.

DeCarlo, E.H., D.J. Hoover, C.W. Young, R.S. Hoover, and F.T. Mackenzie, 2007. Impact of storm runoff from tropical watershed on coastal water quality and productivity. *Applied Geochemistry* 22(8):1777–1797.

Durski, S.M., S.M. Glenn, and D.B. Haidvogel, 2004. Vertical mixing schemes in the coastal ocean: Comparison of the level 2.5 Mellor-Yamada scheme with an enhanced version of the K profile parameterization. *Journal of Geophysical Research: Oceans*, *109*(C1).

Egbert, G.D., A.F. Bennett, and M.G. Foreman, 1994. TOPEX/POSEIDON tides estimated using a global inverse model.

Giambelluca, T.W., Q. Chen, A.G. Frazier, J.P. Price, Y.-L. Chen, P.-S. Chu, J.K. Eischeid, and D.M. Delparte, 2013. Online Rainfall Atlas of Hawai‘i. *Bull. Amer. Meteor. Soc.* 94, 313-316, doi: 10.1175/BAMS-D-11-00228.1

Hearn, C.J. and M.J. Atkinson, 2001. Effects of sea-level rise on the hydrodynamics of a coral reef lagoon: Kaneohe Bay, Hawaii. *Ocean and Atmosphere Pacific: OAP*, *95*, pp.25-477.

Jones, G.P., M.J. Milicich, M.J. Emslie, and C. Lunow, 1999. Self-recruitment in a coral reef fish population. *Nature*, *402*(6763), pp.802-804.

Lobel, P.S. 1989. Ocean current variability and the spawning season of Hawaiian reef fishes. *Environmental Biology of Fishes*, *24*(3), pp.161-171.

Longenecker, K. and R. Langston, 2008. Life History Compendium of Exploited Hawaiian Fishes. *Honolulu, HI.*

Lowe, R.J., J.L. Falter, S.G. Monismith, and M.J. Atkinson, 2009. A numerical study of circulation in a coastal reef-lagoon system. *Journal of Geophysical Research: Oceans*, *114*(C6).

Matthews D., B. S. Powell, and I. Janeković, 2012. Analysis of Four-dimensional Variational State Estimation of the Hawaiian Waters. *Journal of Geophysical Research: Oceans*, *117*(C3).

McManus, M.A. and C.B. Woodson, 2012. Plankton distribution and ocean dispersal. *Journal of Experimental Biology*, *215*(6), pp.1008-1016.

Michalakes, J., S. Chen, J. Dudhia, L. Hart, J. Klemp, J. Middlecoff, and W. Skamarock, 2001. Development of a Next Generation Regional Weather Research and Forecast Model. *Developments in Teracomputing*: Proceedings of the Ninth ECMWF Workshop on the Use of High Performance Computing in Meteorology. Eds. Walter Zwieflhofer and Norbert Kreitz. World Scientific, Singapore. pp. 269-276.

North, E.W., Z. Schlag, R.R. Hood, M. Li, L. Zhong, T. Gross, and V.S. Kennedy, 2008. Vertical swimming behavior influences the dispersal of simulated oyster larvae in a coupled particle-tracking and hydrodynamic model of Chesapeake Bay. *Marine Ecology Progress Series*, *359*, pp.99-115.

North, E.W., E. Adams, Z.Z. Schlag, C.R. Sherwood, R.R. He, K.H.K. Hyun and S.A. Socolofsky, 2011. Simulating oil droplet dispersal from the Deepwater Horizon spill with a Lagrangian approach. *Monitoring and Modeling the Deepwater Horizon Oil Spill: Record-Breaking Enterprise*, pp.217-226.

O'Connor, M.I., J.F. Bruno, S.D. Gaines, B.S. Halpern, S.E. Lester, B.P. Kinlan, and J.M. Weiss, 2007. Temperature control of larval dispersal and the implications for marine ecology, evolution, and conservation. *Proceedings of the National Academy of Sciences*, *104*(4), pp.1266-1271.

Ostrander, C.E., M.A. McManus, E.H. DeCarlo, and F.T. Mackenzie, 2008. Temporal and Spatial Variability of Freshwater Plumes in a Semienclosed Estuarine–Bay System. *Estuaries and Coasts* 31:192–203, DOI 10.1007/s12237-007-9001-z

Paris, C.B., J. Helgers, E. Van Sebille, and A. Srinivasan, 2013. Connectivity Modeling System: A probabilistic modeling tool for the multi-scale tracking of biotic and abiotic variability in the ocean. *Environmental Modelling & Software*, *42*, pp.47-54.

Pfeiffer-Herbert, A.S., M.A. McManus, P.T. Raimondi, Y. Chao, and F. Chai, 2007. Dispersal of barnacle larvae along the central California coast: a modeling study. *Limnology and oceanography*, *52*(4), pp.1559-1569.

Randall, J.E. 1961. A contribution to the biology of the convia surgeonfish of the Hawaiian Islands, Acanthurus triostegus sandvicensis. *Pacific Science*, *15*(2), pp.215-272.

Sale, P.F. 1991. *The ecology of fishes on coral reefs*. Academic Press.

Shchepetkin, A.F. and J.C. McWilliams, 2005. The regional oceanic modeling system (ROMS): a split-explicit, free-surface, topography-following-coordinate oceanic model. *Ocean Modelling*, *9*(4), pp.347-404.

Schemmel, E.M. and A.M. Friedlander, 2016. Working with fishers to understand temporal and spatial variability in reproductive characteristics of the convict tang (*Acanthurus triostegus sandvicensis*). Manuscript in preparation.

Talbot R. 2014. “Biblical” Spawning Event on Hawaiian Reefs. *Coral Magazine*. http://www.reef2rainforest.com/2014/08/29/biblical-spawning-event-on-hawaiian-reefs/

Thyng, K. M., and R.D. Hetland, 2014. TracPy: Wrapping the Fortran Lagrangian trajectory model TRACMASS, Proceedings of the 13th Python in Science Conference (SCIPY 2014), pp. 85-90

USGS, 2016. USGS Water Services. http://waterservices.usgs.gov/

Warner, J.C., W.R. Geyer, and J.A. Lerczak, 2005. Numerical modeling of an estuary: A comprehensive skill assessment. *Journal of Geophysical Research: Oceans*, *110*(C5).

Willmott, C.J., 1981. On the validation of models. *Physical geography*, *2*(2), pp.184-194.